Russian Geology and Geophysics © 2019, V.S. Sobolev IGM, Siberian Branch of the RAS
Vol. 60, No. 12, pp. 1425–1443, 2019 *DOI:10.15372/RGG2019108* *Geologiya i Geofizika*

High-Grade Metamorphism and Anatexis in the Teletskoe–Chulyshman Belt (Gorny Altai): U–Pb Geochronology, *P–T* Estimates, and Thermal Tectonic Model[1]

O.P. Polyansky[a, ✉], S.A. Kargopolov[a,b], A.V. Babichev[a], V.V. Reverdatto[a]

[a]*V.S. Sobolev Institute of Geology and Mineralogy, Siberian Branch of the Russian Academy of Sciences, pr. Akademika Koptyuga 3, Novosibirsk, 630090, Russia*

[b]*Novosibirsk State University, ul. Pirogova 2, Novosibirsk, 630090, Russia*

Received 15 August 2018; received in revised form 15 February 2019; accepted 21 march 2019

Abstract—A model of the formation of the Teletskoe–Chulyshman metamorphic belt (TCMB) in Gorny Altai has been elaborated. The estimated pressure (not exceeding 3–4 kbar) and temperature (about 740 ºC) indicate an increased regional crustal thermal gradient equal to 60–90 ºC/km during the formation of the metamorphic belt. The age of migmatites of the Chulyshman complex has been evaluated at 483.9 ± 5.7 Ma (Early Ordovician) by U/Pb (SHRIMP) zircon dating. The paleogeodynamic setting of the TCMB formation and the protolith nature are identified based on the geochemical and petrochemical parameters of the metamorphic rocks. Structural parameters and numerical modeling show that the Chulyshman migmatite–gneiss complex is an apical part of the thermal-dome structure formed under the thermal impact of a magmatic basic heat source in the base of the crust and displaced to the relevant depths via thrusts and crustal extrusion during the Early Ordovician accretion–collision event. Matching the metamorphism parameters and the numerical-modeling results for the crustal thermal regime, we determined the rate of the anatectic front displacement along the thrust to be at least 6 cm/yr.

Keywords: P–T parameters, thermal tectonic model, U/Pb age, high-temperature/low-pressure metamorphism, Teletskoe–Chulyshman metamorphic belt, Gorny Altai

INTRODUCTION

When it comes to formation of collisional orogens, the nature of anomalous heat flux and the resulting high-grade metamorphism and anatexis is among the key problems. The Teletskoe–Chulyshman metamorphic belt (TCMB) located at the interface of the Gorny Altai and Sayan–Tuva folded systems (Shokalskii et al., 2000; Buslov et al., 2003, 2013; Nokleberg, 2004) is one of the largest manifestations of these processes in the Altai–Sayan folded area (Gusev, 2013; Kargopolov et al., 2016). This metamorphic belt consists of three parts, namely Chul'cha, Chulyshman, and Mogen–Buren blocks (Gusev, 2013), which are understudied in terms of the metamorphism nature, protolith composition, and causes of thermal events during the formation of the accretional-collisional structure of Gorny Altai (Kruk et al., 2013). The age range of the TCMB formation remains unidentified as well, with only isolated dates of metamorphic rocks and primarily intrusive formations outside the TCMB available to presumably limit the age of metamorphic processes (Rudnev et al., 2004; Glorie et al., 2011; Gusev, 2013).

The available estimates of PT parameters based on investigation of a significant volume of petrographic data (Kargopolov et al., 2016) show that the complex was formed under conditions of high-grade metamorphism. To identify the causes of high-grade metamorphism and anatexis at moderate depths (high temperatures/low pressures, HT/LP), we developed a 2D numerical thermal-mechanical model. The problem of the thermal source of metamorphism, anatexis, and migmatization front propagation was stated based on the data on the presence of basic magmas in the collisional orogenic crust (Johnson and Harley, 2012; Brown, 2013). The numerical model, which explains the formation of deeply metamorphosed fragments of the continental crust during collision, is a modified collisional metamorphism and subduction model developed in (Likhanov et al., 2004; Korobeynikov et al., 2008, Korobeinikov et al., 2006, 2012, Polyansky et al., 2010, 2015).

The required research was performed to validate the problem statement, the choice of boundary and initial conditions, and the development of the thermal-mechanical model which included the following: (1) Determination of the paleogeodynamic setting of the TCMB formation and the protolith nature based on geochemical parameters and whole-rock chemistry of metamorphic rocks, (2) Estimation of *P–T* parameters and a possible thermal source of metamorphism,

[1]This paper was translated by the authors.

✉ Corresponding author.
E-mail adress: pol@igm.nsc.ru (O.P. Polyansky)

(3) Dating of the peak metamorphism, which caused anatexis and migmatization based on U/Pb ages in zircon, (4) Characterization of folding types in the belt and its specific blocks listed above, which determine the tectonic control of the TCMB formation. With all these data available, a correct thermal-mechanical evolution model may be developed for the metamorphic belt.

In the following sections of the paper, major and trace element composition of rocks are described, *P–T* parameters of metamorphism are estimated, and the new results of U–Pb dating of zircons from migmatites of the Chulyshman complex within the TCMB are presented; in the last section, the numerical thermal-chemical model is described and the modeling results are presented.

TECTONIC SETTING

The studied metamorphic belt is attributed by various authors to Gorny Altai (Blyuman, 1985; Gusev, 2013), West Sayan–Tuva folded area (Shokalskii et al., 2000; Nokleberg et al., 2004) or is considered a margin of the Altai–Mongolian terrain (Buslov et al., 2003; Buslov, 2011) (Fig. 1*a*). The belt is bounded from southwest and northeast by Teletskoe–Bashkaus and Shapshal collisional fault zones, which separate the Gorny Altai, Teletskoe, and West Sayan terranes (Vladimirov et al., 2008). Regardless of the attribution, it is generally accepted that the belt was formed at the Early Ordovician accretion-collision stage, which reflects the attachment of perioceanic and island arc systems to the edge of the Siberian continent (Kruk, 2015 and references therein). Metamorphic complexes of the belt are represented by the Chul'cha, Chulyshman, and Mogen-Buren blocks (Gusev, 2013) (Fig. 1*b*). Granitoids that penetrate metamorphic rock are considered Early or Middle Devonian (Shokalskii et al., 2000; Kruk, 2015), while the metamorphic complexes themselves were not dated precisely and are approximately aged PR_2–PZ_1 (Shokalskii et al., 2011). Metamorphism age in one of the complexes, namely Chul'cha, was identified in (Gusev, 2013). Several age clusters were obtained from migmatized garnet-sillimanite-biotite gneisses of the complex based on zircon. Detrital grains showed the early Vendian age of 586–583 Ma, while the Early Ordovician concordant age of 466.7 ± 3.3 Ma was determined for most metamorphic rims of zircons (29 measurements, precise sample locations not indicated). According to (Gusev, 2013), the upper age boundary of protolith deposition for Chul'cha gneisses was identified as Early Ordovician and the age of metamorphism as Middle Ordovician. The other metamorphic complexes of the eastern Gorny Altai are identified as Neoproterozoic–early Paleozoic depositions transformed during the later thermal-tectonic processes (Kruk et al., 2013). The Bashkaus and Kurai metamorphic blocks located to the southwest of the TCMB are separated by tectonic interfaces and differ from the latter in the degree of metamorphism. Their age ranges were established based on U–Pb ages in individual zircon grains, which makes them quite approximate. The greenschist metamorphism of the Bashkaus complex is dated as post-middle Cambrian based on the age of detrital zircons; the study failed to identify the upper age boundary (Gusev, 2013). Synkinematic granitoids of the axial part of the Tongulak Ridge within the Kurai metamorphic block were identified by U–Pb isotopic dating of zircons as Late Ordovician at 444 ± 17 Ma (Kruk et al., 2004). The age of migmatized kyanite-sillimanite-biotite gneisses within the same block was identified based on individual metamorphogenic zircon grains at 443 ± 9.5 and 422.9 ± 9.1 Ma (Gusev, 2013). During the formation of the Tongulak zonal metamorphic complex, a thermal source seems to be represented by a basic, uneroded intrusion (Ananiev et al., 2003).

Previous Ar–Ar datings of biotite from tectonites of the Teletskoe–Bashkaus fault zone (middle course of the Chulyshman River, Katuyaryk locality) show the age range of 343–309 Ma (Buslov et al., 2003). These boundaries are associated with the late early Carboniferous stage of fault reactivation along the Teletskoe–Bashkaus and Shapshal fault zones and not related to high-temperature metamorphism events.

Thus, the Ordovician stages (467–443 Ma) identified for a series of metamorphic complexes in the east of Gorny Altai are characterized by andalusite-sillimanite metamorphism of epidote-amphibolite and amphibolite facies and match the final formation stage of the structures of Gorny Altai (Vladimirov et al., 2008). The information regarding TCMB is limited since no detailed research of rock composition, metamorphism conditions and thermal event ages were performed.

Structural analysis of folded areas

As mentioned above, Chul'cha, Chulyshman, and Mogen-Buren are the three blocks distinguished within the TCMB (Shokal'skii et al., 2011). Based on the analysis of folded structures, the data on rock texture, metamorphism parameters, and major and trace element composition, we may answer a pivotal question of whether these blocks represent different complexes in terms of deposition basin type and postdeposition metamorphism and folding, or they are tectonically separated parts of the same metamorphic belt. Based on the assessment of metamorphism conditions and geochronological data, we may assume that the metamorphic complex was formed at indivisible stage. It should be emphasized that its current structure and position within the present tectonic collage, as well as exhumation history (possibly comprising multiple stages), is beyond the scope of the present paper and is considered in (Dobretsov et al., 2017).

In this section, we consider the description of folding of metamorphic rocks in various blocks. Description of sin-metamorphogenic folding is useful for estimating the kinematics of tectonic displacements associated with metamorphism and formation of the internal structure of the Teletskoe–Chulyshman belt.

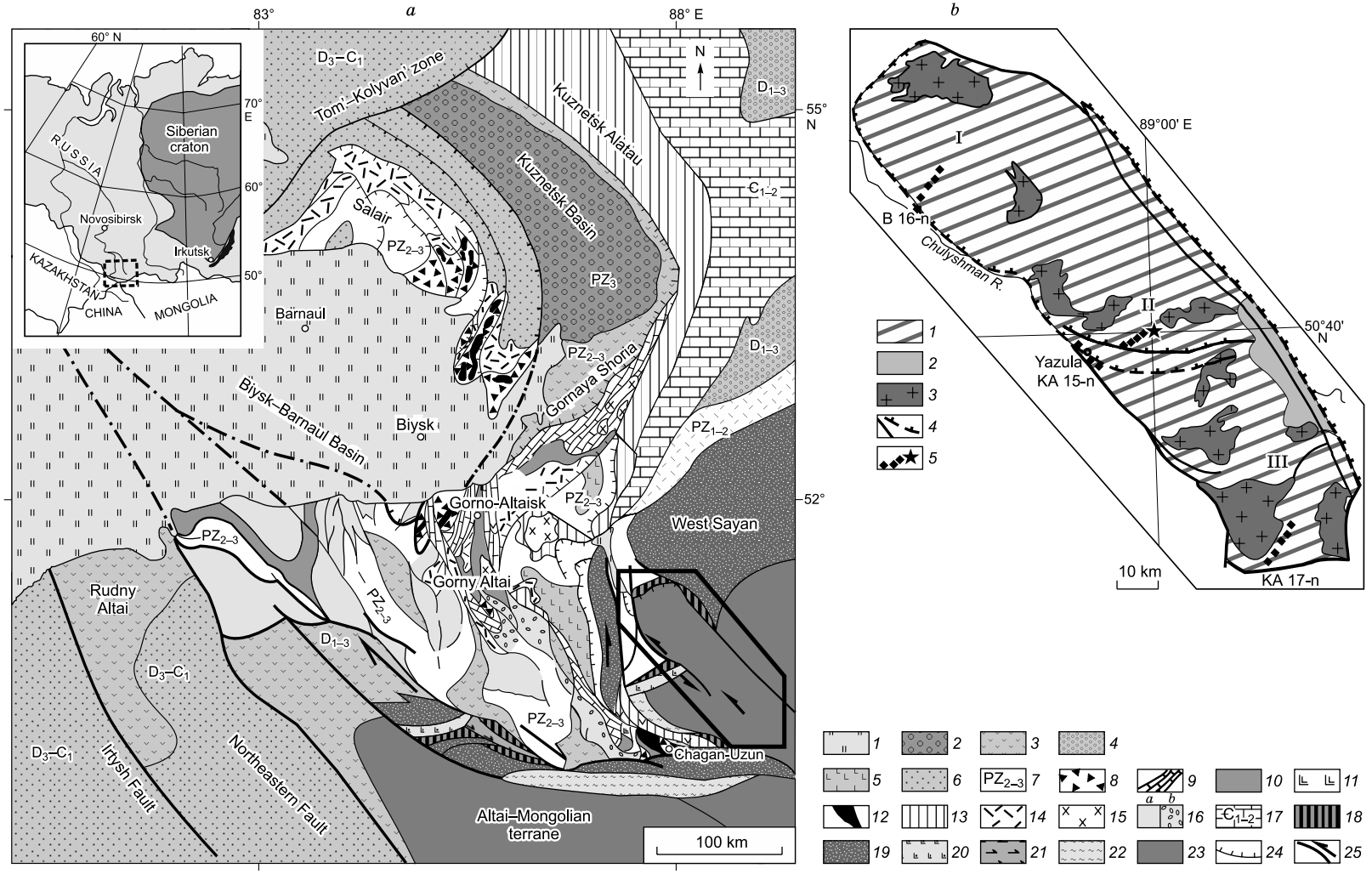

Fig. 1. *a*, Geological and geodynamic scheme of the Gorny Altai and adjacent areas, according to (Dobretsov et al., 2017). *1*, Biysk–Barnaul Cenozoic depression; *2*, Permian–Mesozoic formations of the Kuznetsk Basin; *3–16*, marginal-continental complexes of the Siberian continent: *3–6*, Devonian–early Carboniferous active margin: magmatic arc (*3*), sedimentary complexes of the back-arc basin (*4*), rhyolite-basalt complexes of the back-arc basin (*5*), volcanosedimentary rocks of the back-arc basin (*6*); *7*, Ordovician–Early Devonian passive margin; *8–12*, Vendian–Early Ordovician active margin: *8*, olistostromes, *9–12*, paleo-oceanic crust: carbonate "caps" of the paleo-oceanic island (*9*), volcanosedimentary formations of the paleo-oceanic island (*10*), basalt-siliceous rocks of the oceanic bottom (*11*), ophiolites (*12*); *13–16*, Vendian–Early Ordovician Kuznetsk–Altai island arc: tholeiite-boninite series (*13*), calc-alkaline series (*14*), Cambrian gabbroids (*15*), middle Cambrian–Early Ordovician Anyui–Chuya forearc through (*16*): *a*, turbidites, *b*, olistostrome-conglomerate formations of the coastal zone; *17*, early–middle Cambrian carbonate-terrigenous rocks of the back-arc basin; *18–21*, middle–late Paleozoic Charysh–Terekta–Ulagan suture-shear zone: Cambrian and Early Ordovician ophiolites (*18*), early Paleozoic turbidities (*19*), Cambrian and Early Ordovician complexes of paleo-oceanic islands (*20*), Ordovician blueschists (*21*); *22–25*, complexes of the Kazakhstan–Baikal composite continent: South Chuya and Kurai middle Paleozoic metamorphic complexes (*22*), early Paleozoic turbidites of the Altai–Mongolian terrane (*23*), middle Paleozoic thrusts (*24*), late Paleozoic strike-slips (*25*). The polygon shows the position of the complex under study. *b*, Structure of the Teletskoe–Chulyshman metamorphic belt. Roman numerals denote metamorphic blocks: I, Chul'cha; II, Chulyshman; III, Mogen-Buren. *1*, Teletskoe–Chulyshman metamorphic belt (TCMB); *2*, Quaternary sediments; *3*, Early–Middle Devonian granitoids, undifferentiated; *4*, strike-slips (solid) and thrusts (figured lines); *5*, sampling profiles: KA15-n ("Yazula"), B16-n ("Chulcha"), KA17-n ("Buguzun"), star—the sampling point KA14-3/3 for age dating (50°39.42′ N; 88°54.90′ E).

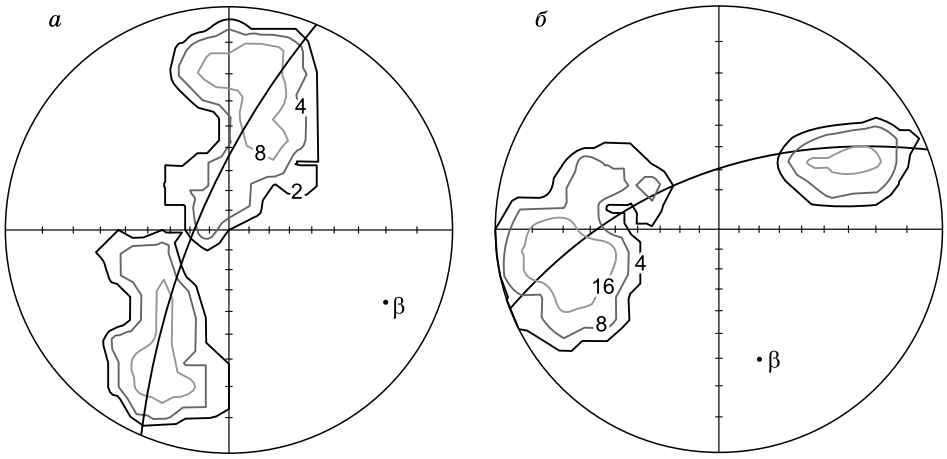

Fig. 2. Stereographic projections of poles of planar elements of bedding (migmatitic foliation, schistosity) are shown on the lower hemisphere for the different areas of metamorphic belt (equiangular projection). β is the calculated position of the mean hinge. The position of the fold belt is indicated by the arc of a great circle. *a*, Cordierite migmatites and shales of the Yazula area. Isolines are drawn for 2–4–8% observation density. The total number of observations is 61. Orientation of the fold belt is 73/294, β 17/114. *b*, Cordierite migmatites and shales of the Buguzun area: Isolines are drawn for 4–8–16% measurement density; orientation of the fold belt is 62/339; orientation of β is 28/159; n = 38. Data processing was carried out in the GEOrient.9.5.1 package (Holcombe, 2015).

Orientations of planar (migmatite banding and foliation) and linear (small-scale fold bends) elements were measured in three sites, i.e., along profiles B-16 (Chul'cha), KA15-n (Chulyshman), and KA17-n (Mogen-Buren, near the Buguzun Pass, Chikhachev Ridge) (Fig. 1*b*). Nonuniform sampling density was primarily due to wide-spread moraine development. There were only 10 banding measurements taken in the Chul'cha block, and therefore it is not considered in the present paper. However, it should be noted that in terms of symmetry the distribution of individual points completely matches that of the Chulyshman block. Stereographic projections of poles of planar elements of bedding for two reference sites within the metamorphic belt located within 70–80 km from each other, which characterize the central and the southern parts of the belt (Fig. 1*b*), are shown in Fig. 2.

In both sites, cylindrical folding with steeply dipping axial planes is recognized. The total sampling area for the KA15-n profile reaches several dozen square kilometers. Here, an average hinge dips along the SE direction at an angle of 17º (Fig. 2*a*). For the zones with maximum observation density (with isoline over 8%), the angle between the limbs in the basic structural motif is *c*. 40º–50º.

Folding geometry in the southern part of the KA17-n profile is close to that for the central part (KA15-n). The calculated hinge also dips in the SE direction, but the dip angle is slightly higher, specifically by 28º. Here, the interlimb angle is close to that in the previous example, i.e., about 40º. At the same time, the hinges have different dip azimuths, i.e., the latter is rotated to the north by 50º–60º. These variations in positions of axial planes/hinges may be due to natural virgation during folding. The possibility of the tectonic (fault-based) relative rotation during the subsequent processes is not to be discarded as well.

The synchronism of metamorphism and deformations is explained by their shared structural-metamorphic paragenesis (Miller, 1982) and signs of syn-kinematic mineral growth (Passchier and Trouw, 2005).

Migmatite banding in the studied complex is impacted by folding (Fig. 3*a*), and both the leucosome and melanosome include identical mineral (Q + Pl ± Kfs) + Crd + Sill + Bt + Sp assemblages. Foliation and banding are formed by biotite, sillimanite, and cordierite. This is true for both individual grains and their lenticular-shaped aggregates. Banding orientation is also expressed by the presence of individual flattened grains and quartz segregation. Orientation of small-scale fold hinges is emphasized by elongations of biotite and sillimanite grains, as well as fibrolite aggregates. Thus, minerals and their aggregates were formed in a syn-kinematic fashion and are located within a single structural-metamorphic paragenesis. Cordierite shows clear signs of mimetic crystallization (Fig. 3*b*). Orientation of sillimanite inclusions in the helicitic cordierite structure fully matches positions of planar textures (Fig. 3*c*).

Thus, uniform linear folding with a cylindrical motif is observed throughout the whole Teletskoe–Chulyshman belt. The key finding of the stereographic projection analysis is that the structural motif of the TCMB is determined by linear folding formed simultaneously with peak metamorphism. The folding type makes it possible to consider NE-SW the prevalent trend of compressional deformations throughout the whole Teletskoe–Chulyshman belt.

Whole-rock chemistry in the Teletskoe–Chulyshman metamorphic belt

The research took place in the southwestern part of the Chul'cha complex (B16-n profile), in the central part of the Chulyshman complex near the Yazula Village (KA15-n profile), and in the southern part of the Mogen-Buren complex

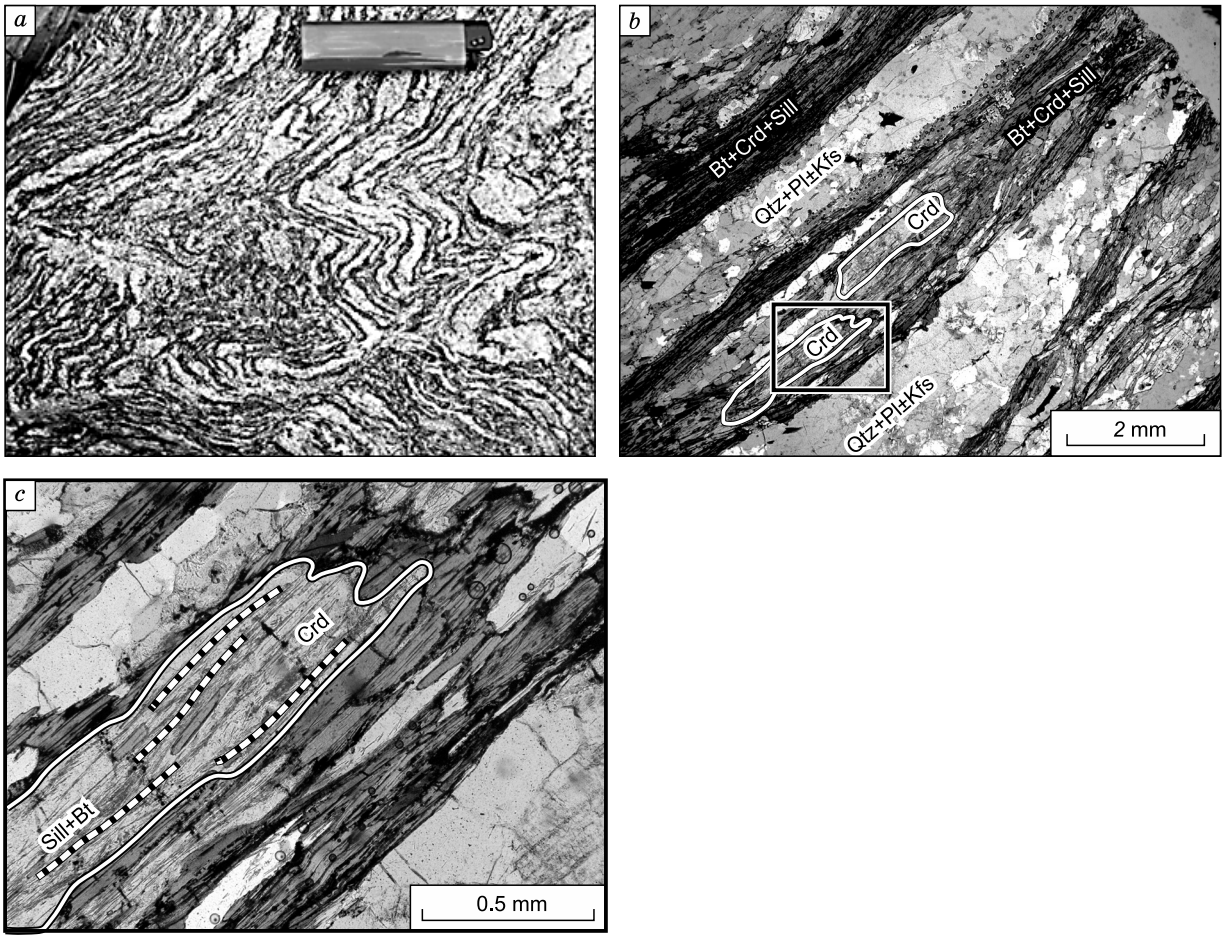

Fig. 3. Metamorphic foliation in rocks of the TCMB (KA15-n profile, Chulyshman block). *a*, Migmatitic folding in the outcrop. *b*, Same in thin section KA14-3-5. Assemblage of Qtz + Pl ± Kfs prevail in the leucosome, assemblage of Bt + Crd + Sill/Fib + Sp prevail in the melanosome. Scale bar is 2 mm (the rectangle shows the micrograph in Fig. 9*c*). *c*, Cordierite porphyroblasts elongated in the plane of banding with heliocyte structure made with sillimanite/fibrolite and fine-grained biotite are shown. Scale bar is 0.5 mm. Hereinafter: Bt, biotite; Crd, cordierite; Sil, sillimanite; Qtz, quartz; Ilm, ilmenite; Kfs, K-feldspar; Pl, plagioclase; Phl, phlogopite; Mgt, magnetite; Ms, muscovite; Als, aluminosilicate; Opx, othopyroxene; Grt, garnet; L, melt; V, volatile; Opq, opaque.

(KA17-n profile, Fig. 1*b*) with samples and rock bedding elements collected along the profiles of 10–20 km long.

Bulk-rock composition. To determine the paleogeodynamic setting of protolith formation for metamorphic rocks and migmatites, the standard studies of whole-rock major and trace elements compositions were performed. The studied section of the Teletskoe–Chulyshman complex is represented by metapelite sequence uniform in composition. Occasional Bt-Amp-schists are observed locally.

Based on sodium-silicate modulus values ($(Na_2O + K_2O)/Al_2O_3$) of 0.2–0.53 (0.31 for muscovite), the protolith could include the rocks with primary contents of K-feldspar and overall low degree of chemical weathering (Yudovich and Ketris, 2000). The average hydrolysate modulus (HM) value was 0.40. Thus, based on the mentioned critical indicator relations, the protolith may generally be diagnosed as normal sialites with prevalence of sand-silt and clayey rocks (Yudovich and Ketris, 2000).

The majority of protolith composition points in the Herron classification diagram (Herron, 1988) fall within the argillaceous field (Fig. 4*a*). Here, multidimensional statistical processing of the data available made it possible to identify three stable groups of rocks at the coordinates of major elements. A stable grouping like this may indicate multiple provenances of the sediments. Uniform distribution of data points corresponding to groups with different compositions across the studied area confirms the presence of a common metamorphic complex.

An attempt at estimating provenance fields is shown in Fig. 5*b* (Roser and Korsch, 1988). As expected, the data points mostly fall within the redeposited felsic sediments field and partly within the field of erosion products of felsic magmatic formations.

The maturity of sediments is well illustrated by the A–CN–K diagram (Fig. 5*c*) with the additional CIA axis (Nesbitt and Young, 1982; McLennan et al., 1993). The weathering

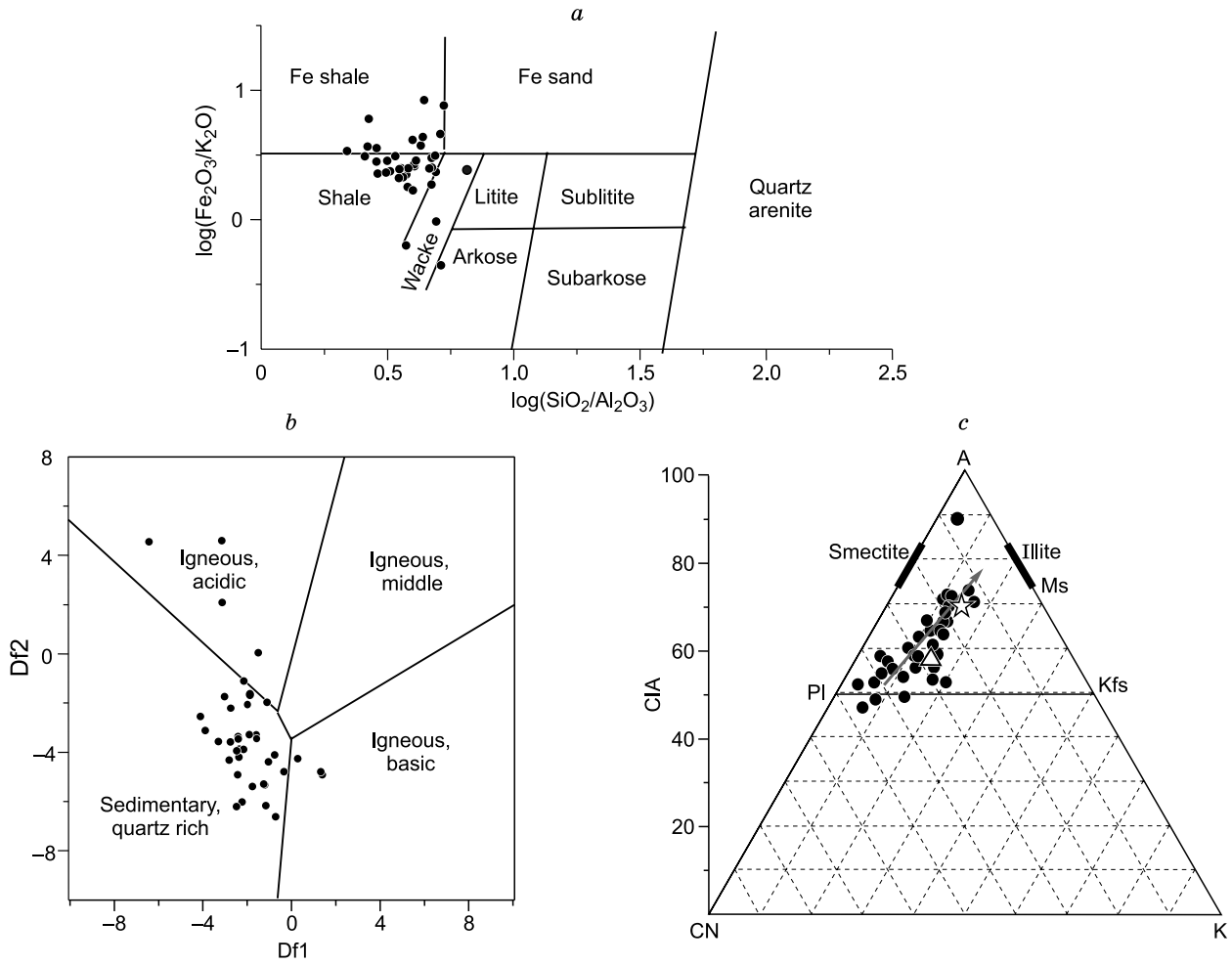

Fig. 4. *a*, Herron diagram (Herron, 1988) for metamorphic rocks of the Teletskoe–Chulyshman metamorphic complex; *b*, Discrimination diagram after (Roser and Korsch, 1988) for metapelites of the Teletskoe–Chulyshman complex; *c*, A–CN–K (CIA) diagram after (Nesbitt and Young, 1982; McLennan et al., 1993). A = Al_2O_3; CN = CaO* + Na_2O; K = K_2O. The chemical index of weathering is CIA = $Al_2O_3/(Al_2O_3 + K_2O + Na_2O + CaO^*)\cdot 100$. All coordinates in the diagram are in molecular quantities. The asterisk is PAAS, the triangle is NASC.

trend extends from the line of unchanged feldspars towards illites. In general, data points corresponding to standard argillaceous shales NASC (Gromet et al., 1984) and PAAS (Taylor and McLennan, 1985) are attributed to the trend line as well. Based on the data available, we may assume that the protolith of the studied metamorphic sequence is represented by sediments with weak degree of differentiation.

Assessment of the geodynamic setting of the sedimentary basin origin from the perspective of thermal modeling of metamorphism is of interest in the present paper. There are reasons to assume that formation of the sedimentary sequence and high-grade metamorphism are rather closely spaced in time and have a certain genetic relation. In particular, this assumption is confirmed by the diagram (Roser and Korsch, 1986), where the whole metapelite sample set matches the field of active continental margins and island arcs. Similar settings are confirmed by the data on trace and rare earth element compositions (see below). Overall, it should be accepted that the rocks of the Teletskoe–Chulyshman complex match the metapelites of the metamorphic complexes of Gorny Altai in terms of their major elements composition (Kruk et al., 2013).

Trace element chemistry. Data on the contents of trace and rare earth elements in the metapelite samples from the Teletskoe–Chulyshman complex are presented in Table 1. REE contents in metapelites vary rather significantly (134–222 ppm) reaching the levels typical for Post-Archean Argillaceous Shales (PAAS) (183 ppm), and in some cases even exceeding those. At the same time, the lowest lanthanide contents (86 ppm) are observed in granite (sample KA 15-4/7). Asymmetric distribution spectra of REE in the rocks of the Teletskoe–Chulyshman complex (Fig. 5*a*) look similar and are characterized by moderate fractionation with the prevalence of light REE over heavy ones ($(La/Yb)_n$ = 4.5–10.0) and pronounced Eu minimums (Eu* = 0.51–0.91). No clear dependence is observed between $(La/Yb)_n$ and total REE contents.

Table 1. Contents of REE and trace elements (ppm) in representative samples from the Chulyshman, Chul'cha and Mogen-Buren blocks of the TCMB

Element	KA 13-2/3	KA 14-3/3	KA 14-3/7	KA 15-4/7	KA 15-7/4	B 16-1	B 16-2	B 16-8	B 16-23	B 16-25	KA 17-1/9	KA 17-1/11	KA 17-2/2	KA 17-2/4	KA 17-2/6
Sc	22	20	30	4.4	23	14.3	35	14.8	18.8	16.1	14.9	23	14.5	18.5	17.1
V	141	131	186	18.5	151	115	174	127	119	127	104	146	95	124	119
Cr	186	181	263	34	245	228	380	232	343	192	321	306	256	331	295
Co	24	25	30	2.1	30	18.3	30	19.5	22	22	16.8	21	17.1	21	20
Ni	97	105	131	4.1	164	97	131	101	117	96	107	119	87	130	120
Cu	15.6	7.1	25	10.5	50	7.6	14.8	7.7	65	6.2	30	14.8	21	12.2	16.9
Zn	114	99	152	43	85	75	144	82	89	114	173	78	109	122	186
Rb	103	121	147	180	102	87	121	97	75	98	77	147	131	77	63
Sr	127	151	103	117	277	265	177	226	178	133	287	79	251	252	401
Y	34	27	44	13.3	31	21	55	26	29	27	28	36	30	28	26
Zr	167	145	271	151	183	210	242	193	145	170	177	161	159	193	191
Nb	11.7	9.3	14.3	9.8	11.1	9.4	13.6	11.2	8.5	9.9	8.1	10.2	9.4	9.2	8.3
Cs	6.3	7.5	8.2	11.0	7.2	2.9	2.9	2.7	2.2	4.2	3.3	5.3	10.1	2.2	3.2
Ba	444	420	236	384	676	282	510	294	270	316	498	545	644	582	404
La	35	26	43	17.5	31	29	41	35	26	34	28	25	28	30	30
Ce	71	54	89	33	67	59	84	71	53	68	54	51	58	61	60
Pr	8.8	6.5	10.7	4.5	8.0	7.0	10.2	8.9	6.6	8.4	6.6	6.1	7.0	7.3	7.1
Nd	34	25	41	17.5	30	27	40	34	25	33	26	25	26	29	28
Sm	7.1	5.2	8.6	3.7	6.2	5.2	8.0	6.9	5.1	7.0	5.0	5.3	5.3	5.6	5.6
Eu	1.31	1.07	1.52	0.58	1.37	1.46	1.63	1.42	1.28	1.12	1.27	1.21	1.05	1.15	1.26
Gd	6.2	4.4	7.6	2.5	5.5	4.3	7.3	6.0	5.2	6.0	5.1	5.6	5.0	5.5	5.2
Tb	0.97	0.75	1.18	0.40	0.83	0.67	1.26	0.86	0.86	0.86	0.80	0.91	0.80	0.81	0.83
Dy	5.9	4.3	7.1	2.3	5.6	3.6	8.7	4.6	5.3	5.1	4.7	6.1	5.0	5.0	4.9
Ho	1.16	0.93	1.58	0.45	1.13	0.77	1.95	0.93	1.11	0.99	0.96	1.25	0.99	0.94	0.91
Er	3.3	2.6	4.6	1.29	3.1	2.2	6.3	2.4	3.0	3.0	2.8	3.7	3.0	2.7	2.6
Tm	0.54	0.44	0.71	0.20	0.50	0.34	1.00	0.37	0.45	0.48	0.42	0.57	0.45	0.43	0.40
Yb	3.5	2.8	4.7	1.35	3.2	2.1	6.3	2.4	2.8	3.1	2.7	3.8	3.1	2.8	2.7
Lu	0.51	0.42	0.68	0.20	0.45	0.31	0.96	0.37	0.43	0.45	0.40	0.54	0.45	0.41	0.40
Hf	4.4	3.7	7.0	4.3	4.8	5.4	6.6	5.2	3.7	4.5	4.2	4.0	4.0	5.1	5.1
Ta	0.91	0.79	0.91	1.22	0.91	0.65	0.88	0.62	0.54	0.65	0.57	0.76	0.82	0.74	0.60
Pb	20	15.0	12.4	26	15.4	17.7	21	19.2	12.9	15.4	25	11.3	16.7	18.2	14.0
Th	12.5	9.8	16.7	16.6	12.7	10.5	17.2	12.8	9.7	14.6	8.3	10.4	10.5	11.4	12.2
U	3.1	1.90	3.7	2.5	2.5	1.94	2.8	1.88	1.64	2.6	1.93	2.5	1.77	2.2	2.7

Note. Chulyshman block: KA13-2/3, KA14-3/3, KA14-3/7, KA15-4/7, KA 15-7/4; Chul'cha block: B16-1, B16-2, B16-8, B16-23, B16-25: Mogen-Buren block: KA17-1/9, KA17-1/11, KA7-2/2, KA17-2/4, KA17-2/6.

Spider diagrams for metapelites of the Teletskoe–Chulyshman complex show clearly visible negative Ba, Nb, Ta, Sr, P, and Ti anomalies and, on the whole, match the multi-element spectrum for PAAS (Fig. 5*b*), the only difference being the lower degree of differentiation. Compared to Post-Archean Australian Shale (PAAS) (Taylor and McLennan, 1985), the rocks of the complex are characterized by slight depletion in Nb and Ta, which indicates the secondary role in their rock source in case the rock formation is linked to subduction processes. Contents of iron group elements (V, Cr, Ni, Co) effectively concentrating in sedimentary rocks of the clay site show levels typical for Post-Archean argillaceous shales and in some cases above those.

To reconstruct paleogeodynamic deposition settings, Bhatia and Kruk diagrams were used (Bhatia and Kruk, 1986). In these diagrams (Fig. 6), figurative metapelite composition points for the Teletskoe–Chulyshman complex fall within the ensialic island arc field.

Thus, the analysis of distribution of major, trace, and rare earth elements makes it possible to assume that protoliths of the Teletskoe–Chulyshman complex were formed in shallow-water offshore settings, their primary source being represented by the transitional crust with an insignificant participation of the differentiated crustal matter from island arcs.

Assessment of metamorphism parameters. Metamorphic sequence of the studied complex is rather homogeneous

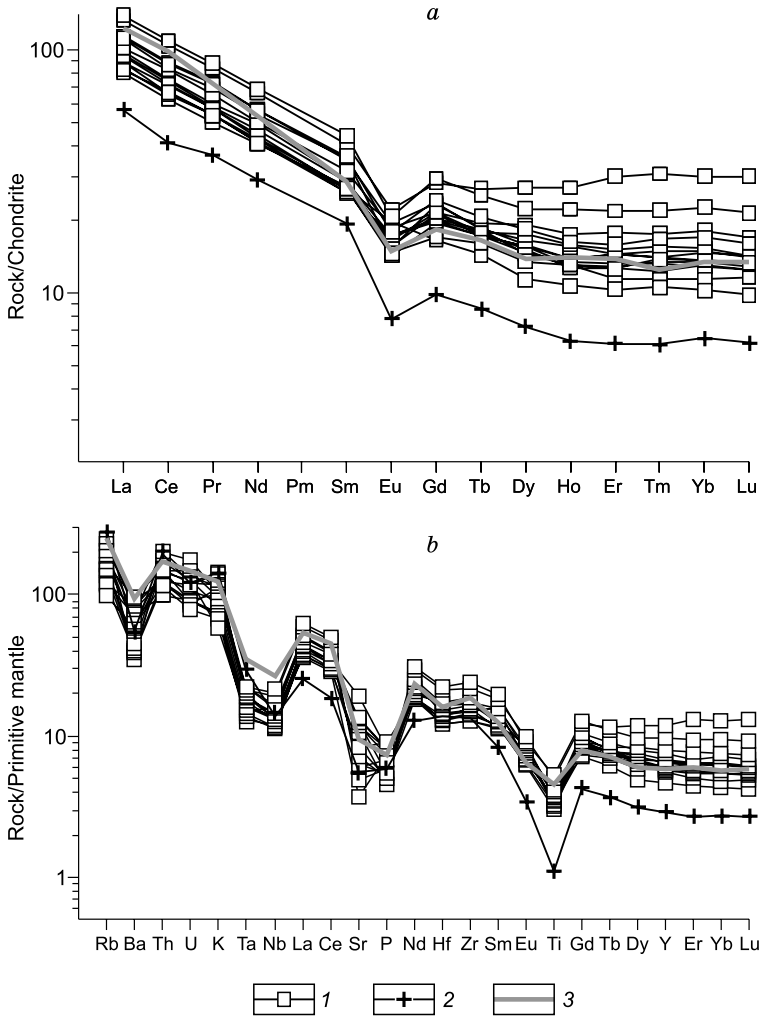

Fig. 5. REE (*a*) and multi-element plot (*b*) of the composition of the metapelite rocks of the Teletskoe–Chulyshman complex. *1,* metapelites; *2*, granites. The bold line (*3*) corresponds to the standard of the post-Archean clay shales PAAS (Taylor and McLennan, 1985).

and is formed by metapelites. These are represented by migmatites (with fine and coarse banding) and by schists. The latter are sometimes characterized by fine banding and foliation with no signs of anatexis. Petrographic differences in rock compositions are primarily manifested in the presence or absence of high-Al minerals, such as sillimanite, andalusite, spinel, and cordierite. The high-Al rock association includes Qtz + Pl + Kfs + Bt + Sil + Crd + Spl + Mag + Ilm. Relatively low-Al rock varieties usually include Qtz + Pl + Bt + Opq ± Kfs. Andalusite is encountered quite rarely. Garnet and primary muscovite are not observed. Cordierite is often euhedral and includes sectorial and polysynthetic twins in thin sections. It is often violet and pure (with no inclusions), with grains reaching 10 cm in diameter. Large grains of this mineral are observed in cordierite granites. As a whole, cordierites are Mg-rich with X_{Mg} values of 0.82–0.65. Metamorphic rocks of the complex have a distinguishing corona texture formed by spinel-cordierite rims around sillimanite.

Maximum temperature values on the petrogenetic grid are determined as follows: association of sillimanite with K-feldspar (see equilibrium lines 1, 2 in Fig. 7); solidus of anatectic migmatites (line 4); absence of orthopyroxene (line 3) and stability of biotite with quartz. In total, this determines the maximum temperature of 700–800 °C. In addition, microprobe study of the composition of all metamorphogenic minerals was performed. All the studies were performed at the Analytical Center for Multielement and Isotope Research SB RAS (Novosibirsk) using a JEOL-JXA-8100 microprobe (analyst V.N. Korolyuk). In particular, compositions of co-existing magnetite and ilmenite were analyzed in the sample KA14-3/3, in which U–Pb absolute age was determined. This allowed us to estimate metamorphism temperature based on Ti distribution between magnetite and ilmenite (Ghiorso and Evans, 2008). A temperature estimate of 740 °C was obtained for minerals with TiO_2 contents of 9.49 and 46.76 wt.% (magnetite and ilmenite, respectively). It should be noted that no exsolution textures typical for regressive metamorphism stage are observed in magnetite.

The minimum pressure at least exceeds 1.5 kbar at T = 740 °C in the sillimanite stability field. A possible maxi-

mum pressure may be determined based on a position of the geotherm corresponding to the gradient of 58 °C/km, which passes through the andalusite field not containing muscovite, below the intersection of curves 1 and 2 (along the pressure axis) since no primary muscovite is observed. The available set of the analyzed minerals (in absence of garnet) does not allow us to obtain precise pressure estimates using the known thermodynamic equilibrium software (for example, THERMOCALC). Based on the identified temperature (about 740 °C) and paleogradient values (58 to 90 °C/km), the possible pressure range of 2.2–3.5 kbar may be estimated, which corresponds to the depths of 8–13 km. Thus, the TCMB is attributed to the andalusite-sillimanite facial series or high-gradient regime under low pressures/high temperatures. The obtained gradient values of 58–90 °C/km are lower, than those for contact metamorphism, and match the maximum values for moderate-pressure metamorphism (Reverdatto and Polyansky, 1992; Reverdatto et al., 2019).

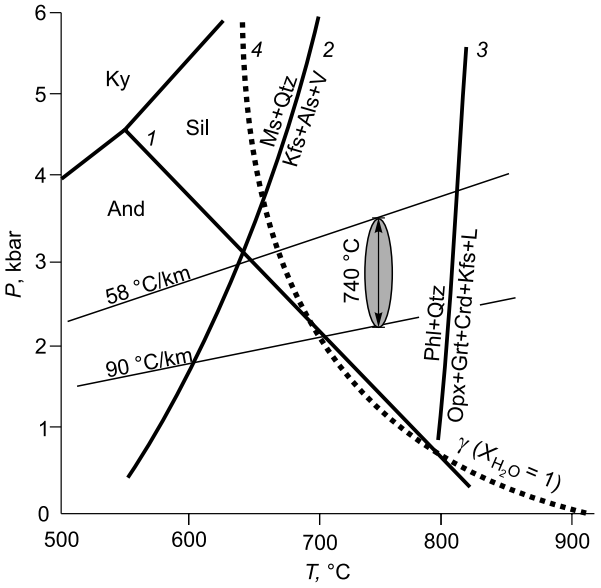

Fig. 7. Petrogenetic grid for metapelites at low pressure/high temperature. The thick vertical line corresponds to the calculated T = 740 °C with the ilmenite-magnetite geothermometer (Ghiorso and Evans, 2008). Equilibrium lines (1–4) are drawn according to (Pattison et al., 2003). The triple point of Al2SiO5 polymorphs is according to (Pattison, 1992). Lines corresponding to the thermal gradients of 58 and 90 °C/km are steady state geotherms for the crust parameters: thermal conductivity of 1.4 W/mK; radioactive heat generation of 1.5 μW/m^3; heat flow of 30 and 60 mW/m^2, respectively; thickness of the heat-generating crust layer of 40 km and 50 km, respectively.

Zircon U/Pb dating of metamorphism

Tectonic contacts with host sequences are a specific feature of the deeply metamorphosed complexes of the TCMB, which makes it difficult to directly correlate them with stratigraphic data. Therefore, identification of the absolute age and correlation of the metamorphic complexes are critical tasks for constructing correct models and event scales for the TCMB formation period. Geochronological studies of the metamorphic complexes of Gorny Altai, as opposed to the magmatic ones, are anecdotal (Glorie et al., 2011; Gusev, 2013; Kruk, 2015).

Zircons for dating were recovered from migmatites of the Chulyshman complex at the location with coordinates 50°39.423′ N; 88°54.889′ E shown in Fig. 1*b*. The sample's mineral assemblage is Qtz + Pl + Kfs + Bt + Sil + Crd + Mag + Ilm. Within the rock, zircons primarily concentrate in cordierite and spinel-cordierite coronas developing along sillimanite.

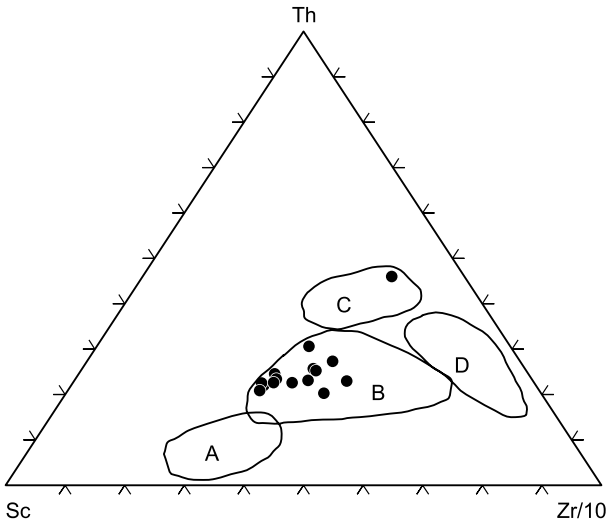

Fig. 6. Sc–Th–Zr/10 discrimination diagram for the metapelite rocks of the Teletskoe–Chulyshman complex. *A*, oceanic island arcs; *B*, continental island arcs; *C*, active continental margins; *D*, passive continental margins, after (Bhatia and Crook, 1986).

Isotopic dating of zircons was performed at the Centre of Isotopic Research of VSEGEI (St. Petersburg). Zircon grains were studied using the SHRIMP-II ion microprobe (analyst P.A. L'vov). U–Pb ages were determined by SHRIMP-II using the technique from (Williams, 1998). Zircon grains were analyzed together with TEMORA and 91500 standard zircon grains (Black et al., 2003). The data were processed using the SQUID software (Ludwig, 2000). The zircons are mostly short columnar grains with a pronounced crystallographic faceting (Fig. 8). Some specimens are football-shaped, while euhedral grains are absolutely prevalent, which is typical for migmatites. No signs of roundness, corrosion, and overgrowth rims were present. Irregular outlines of some grains are due to shearing as a result of sample crushing. Overall, zircons are light and transparent or semitransparent. Fine rhythmic zoning and occasionally sectorial structure can be clearly seen in cathodoluminescent images of the mineral. No signs of detrital zircon were observed in the cores. Black zones in the images (see, for example, 9 and 10) correspond to cavities or inclusions of other minerals, which are clearly visible in reflected or transmitted light.

Table 2. Results of U–Pb ratios determinations in zircons from the leucosome of migmatites of the Chulyshman block

Analysis spot	% $^{206}Pb_c$	U	Th	$^{232}Th/^{238}U$	$^{206}Pb^*$	(1) $^{206}Pb/^{238}U$		$^{238}U/^{206}Pb$	±%	$^{207}Pb/^{206}Pb$	±%	(1) $^{238}U/^{206}Pb^*$	±%	(1) $^{207}Pb^*/^{206}Pb^*$	±%	(1) $^{207}Pb^*/^{235}U$	±%	(1) $^{206}Pb^*/^{238}U$	±%	Err. corr.
		ppm			ppm	Age, Ma														
1.1	0.71	153	54	0.36	10.1	475.1	± 8.8	12.98	1.9	0.0644	3.3	13.07	1.9	0.0586	6.2	0.618	6.5	0.0765	1.9	0.296
2.1	0.50	112	60	0.55	7.5	482.7	± 9.4	12.79	2.0	0.0603	3.4	12.86	2	0.0562	5.6	0.603	5.9	0.0778	2	0.340
3.1	0.61	173	99	0.59	11.2	465.6	± 8.5	13.27	1.8	0.0607	2.8	13.35	1.9	0.0558	5.9	0.576	6.2	0.0749	1.9	0.302
4.1	0.76	194	71	0.38	13.2	486.7	± 8.7	12.65	1.8	0.0619	2.5	12.75	1.9	0.0558	6.3	0.603	6.5	0.0784	1.9	0.284
5.1	0.89	199	74	0.39	13.8	495.1	± 9.1	12.41	1.9	0.0608	3.5	12.52	1.9	0.0535	7.3	0.589	7.6	0.0798	1.9	0.251
6.1	0.92	65	27	0.42	4.3	473	±10	13.02	2.2	0.0661	4.5	13.14	2.3	0.0587	9	0.616	9.3	0.0761	2.3	0.246
7.1	0.88	165	72	0.45	11.4	492.7	± 8.7	12.47	1.8	0.0661	2.2	12.58	1.8	0.0589	6.6	0.645	6.8	0.0794	1.8	0.269
8.1	1.07	122	34	0.29	8.36	487.7	± 9.3	12.58	1.9	0.0658	3.2	12.72	2	0.0571	8.6	0.619	8.8	0.0786	2	0.224
9.1	0.57	218	163	0.77	15	495.3	± 8.7	12.45	1.8	0.0606	3.7	12.52	1.8	0.056	5.5	0.617	5.8	0.0799	1.8	0.314
10.1	0.19	163	117	0.74	10.9	484.2	± 8.4	12.79	1.8	0.0575	3.1	12.82	1.8	0.0559	3.5	0.601	4	0.078	1.8	0.455

Note. For numbers of analysis spots—prefix KA 14-3/3. Errors are given at the 1σ level. Pb_c and Pb*, common and radiogenic lead, respectively. Standard calibration error is 0.54%; (1), common lead corrected using measured ^{204}Pb; Err. corr., correlation coefficient of ratio errors $^{207}Pb^*/^{235}U$ and $^{206}Pb^*/^{238}U$. Analyst P.A. L'vov.

U/Pb dating results are presented in Table 2 and in Fig. 9. The calculated age of migmatites of the southern block of the Teletskoe–Chulyshman belt is 483.9 ± 5.7 Ma (based on ten spots), which fell on the concordance line. The Th/U ratio falls within the interval of 0.29–0.77. This ratio was earlier believed to not exceed 0.1 for the high-degree metamorphic rocks (Rubatto, 2002). However, it was later shown that metamorphogenic zircons may display rather high Th/U values, even above 1.0 (Harley et al., 2007). In our case, zircon did not show any signs of overprinted metamorphic events, and crystallization occurred at the background of partial melting. Concordant position and a slight dispersion of the mean age value indicate that it was a one-act event. The obtained age of migmatites of the Chulyshman complex is then used as a reference point for problem statement, when modeling the HT/LP conditions of metamorphism.

Numerical modeling

Model setup. The model assumes the burial of the metapelite sedimentary protolith to the depth of the lower crust. This burial may be explained by protolith's subduction at an earlier stage. The physical mechanism behind the subsidence of sediments to the depths of 30–40 km as a result of underthrust/subduction was considered earlier by many authors (Dobretsov et al., 2001 and references therein). The model considered is as follows: a basic magma chamber is formed in the thickened crust, which causes heating and anatexis of the host rocks. Then, the convergent motion of the blocks starts, which is accompanied by reverse faulting/thrusting of the tectonic plates. Surface erosion processes during the collision are not taken into account in the present model, i.e., surface topography changes with respect to immobile securely fixed base. In reality however the base of the crust will subside thereby forming mountain roots, and erosion will balance the topography in accordance with isostasy. All these phenomena require special research and dedicated modeling efforts and therefore are not considered in the present paper. This simplification is introduced to solve a particular problem, i.e., explain the mechanism, which causes high temperature/moderate pressure metamorphism, without looking into surface orogeny and denudation processes.

The problem statement, model geometry, boundary and initial conditions are presented in Fig. 10. Modeling was performed in two variants as follows: (a) steeply dipping thrust (b) gently dipping thrust. In both variants the presence of a basic thermal source was assumed, i.e., we consider the thermal impact of a basic magmatic chamber of a complex shape with a width of 30 km and a thickness of 10 km from the base of the crust to the thrust surface. A constant temperature of 1200 °C is maintained in the chamber for 5 Ma. The life span of the basic chamber is determined based on the data on peculiar duration of basaltic magmatism in igneous provinces (Prokoph et al., 2004). The magmatic chamber size (10 × 30 km) is selected similar to the basic intrusion with thickness of 8–9 km and width of >20 km located in the Ivrea-Verbano zone (Alps, North Italy) (Quick et al., 1994). It is assumed that magmatism stops in 5 Ma, which is followed by the allochthon motion with thrusting over the autochthon. Collision rate of the blocks was selected from the interval of 5 to <13 cm/yr, which is typical for Karakoram–Tibet–Himalaya orogeny (Johnson and Harley, 2012).

Kinematic boundary conditions describe the middle Cambrian–Early Ordovician evolution stage of the accretion–collision system of the Gorny Altai orogeny (Buslov et

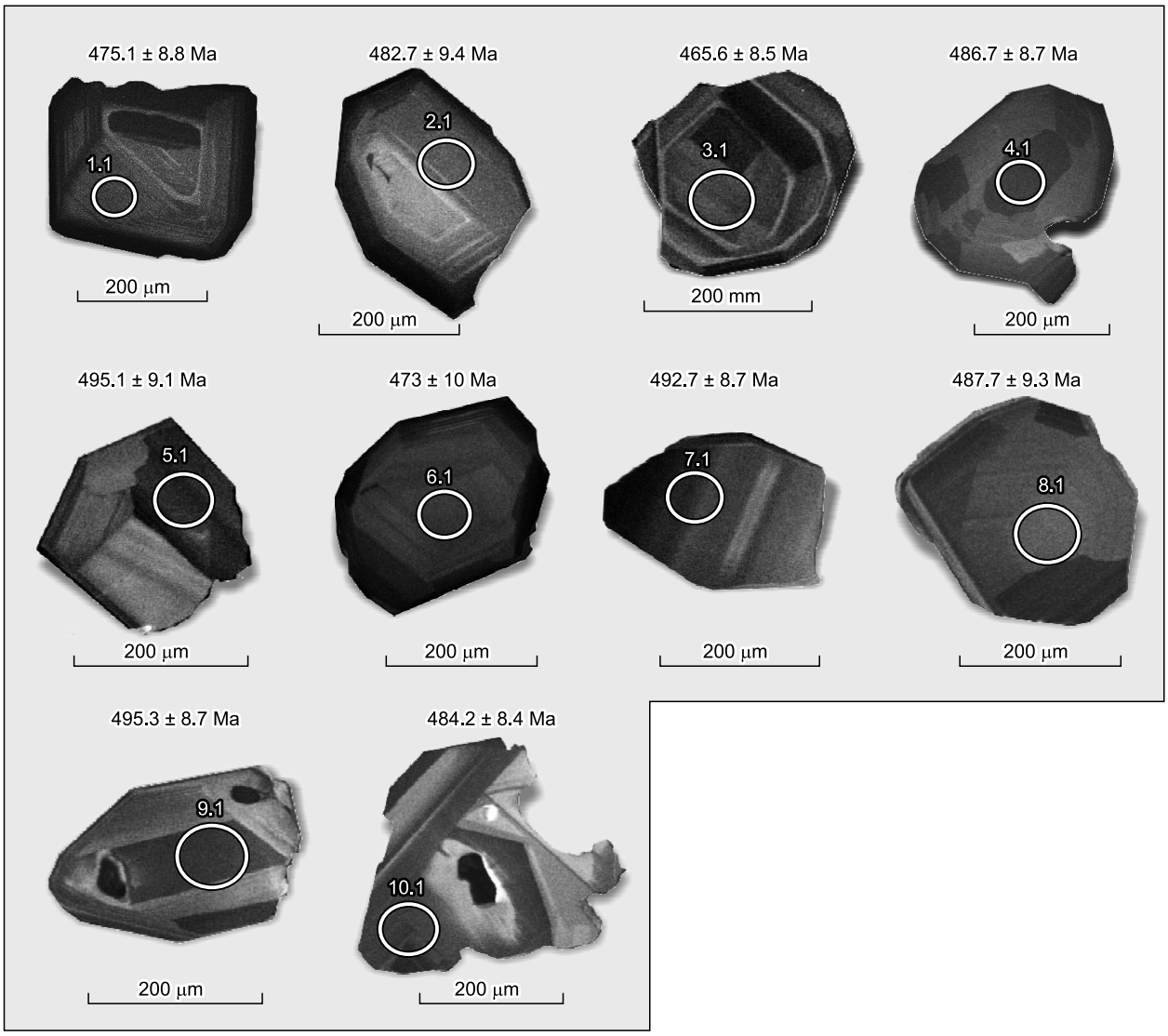

Fig. 8. CL images and U-Pb ages of zircons from migmatites of the Chulyshman complex (sample No. KA14-3/3). White circles indicate points of SHRIMP dating. Numbers of grains correspond to Table 2.

al., 2013; Kruk, 2015). One of the blocks (Gorny Altai) is considered as the autochthon, and the other (West Sayan) moves at a constant rate v (3, 5, 6, and 10 cm/yr in different variants of the model) (Fig. 10). The magmatic chamber is supposed to stay in place the whole time, according to (Quick et al., 1994). Temperature boundary conditions are introduced as constant temperature at the surface (0 °C) and constant heat flux at the lower boundary of the model (Q = 17 mW) under condition of symmetric lateral surfaces. The initial temperature distribution matches the stationary geotherm of the continental crust with the mantle heat flux of 17 mW/m^2; radioactive heat sources not taken into account for the sake of simplicity.

Mechanical properties of the crustal matter are characterized by different rheologies: the Gorny Altai block acts as an inelastic stop and the West Sayan block is described as an elastic-viscous-plastic body. Its properties are set as follows. Plastic properties are described by the Von Mises law with yield stress of σ_Y = 50 MPa. Viscosity is set in accordance with the experimental parameters of wet diorite (Hansen and Carter, 1982) or granite (Ranally, 1995) and is characterized by the behavior of a temperature-dependent non-Newtonian (nonlinear) fluid: $\eta = A^{-\frac{1}{n}}\dot{\varepsilon}^{\frac{1-n}{n}}\exp\left(\frac{H}{nRT}\right)$, where A = 3.01e-16 (Pa^{-n} s^{-1}) is the preexponential constant, n =2.4 is the power-law exponent, and H = 212 (kJ/mol) is the activation energy in the creep law. The other parameters were set as follows: density is 2800 kg/m^3; the Young modulus is E = 100 GPa; the Poisson's ratio is v = 0.25; heat capacity is C_p = 1250 J/(kgK), thermal conductivity is 1.5 W m^{-1}K^{-1}, and the thermal expansion coefficient is α = 1.e-5 K^{-1}.

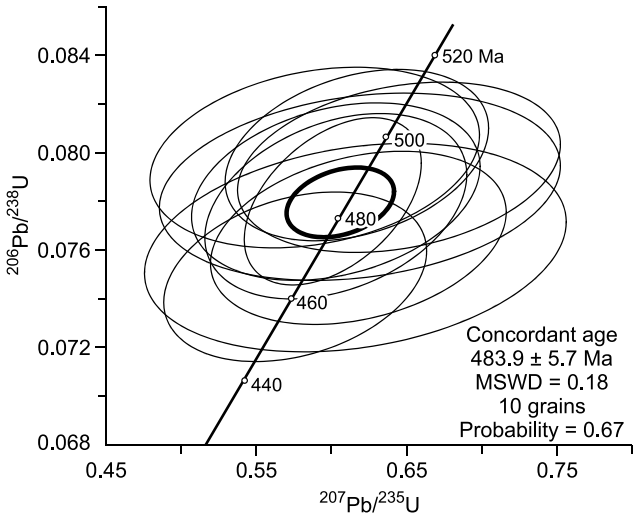

Fig. 9. Concordia plot with SHRIMP data for zircons from migmatites of the Chulyshman complex (sample No. KA14-3/3).

The problem was solved in a 2D configuration, i.e., we considered mechanical equilibrium, heat conductivity, continuity, and constitutive equations, which describe the rheological properties of the material. Phase transition during the melting of the thrusting block (allochthon) is taken into account in momentum and heat balance equations. The solidus temperature of water-saturated granite is set at 650 °C under the pressure corresponding to the middle-lower crust (Johannes and Holtz, 1996), above which viscosity and density match the partial melt properties. Changes in thermal conductivity and heat capacity, as well as the effect of latent heat of melting were not taken into account in the model, due to their weak effects on the heat diffusion compared to advection processes. Detailed derivations of the equations and description of the numerical method employed are presented in (Korobeinikov, 2000; Polyansky et al., 2012, 2014).

Modeling results. Two series of numerical experiments were performed with a steeply and gently dipping fault plane and at different convergence rates of the allochthon and the autochthon of 3, 5, 6, and 10 cm/yr. Thus, we are able to show the effect of geometry and kinematic conditions on temperature regime.

To estimate the maximum temperature and temperature anomaly size at the collision stage, the configuration of the area limited by the isotherm of 700 °C was monitored. The temperature of 740 °C was set as the peak for metamorphic rocks of the Chul'cha block based on mineral associations and accepted as a reference value for model verification. The modeling results are presented in Figs. 11 and 12 for the collision stage of thermal evolution after magmatism termination. Deformation pattern in both series of numerical experiments is characterized by compression and squeezing of the matter upwards. The results of the collision model show that thickening of the crust takes place along with thrusting of the Teletskoe–Chulyshman block over the Gorny Altai block. Inverted temperature distribution in the hanging and foot walls may be observed at the contact area of the blocks. When the movement stops, thermal relaxation occurs for about 20 Ma, i.e., the temperature in the thrusted block decreases and isotherms flatten (the regressive stage is not shown in Figs. 11 and 12). It can be seen from the experiments that the thermal anomaly reaching 700 °C in the crust occurs in both cases, but the temperature field evolution is different.

Evolution of temperature and viscous deformations in the reverse fault model is shown for successive collision stages in Fig. 11. Crustal rocks are heated above the magmatic chamber, partial melting occurs, which leads to a decrease in rock density and gravitational instability of the partially molten body. Low-density masses originate due to anatexis, and, when the collision starts with the convergence velocity of blocks of 5 cm/yr, the partially molten body is detached

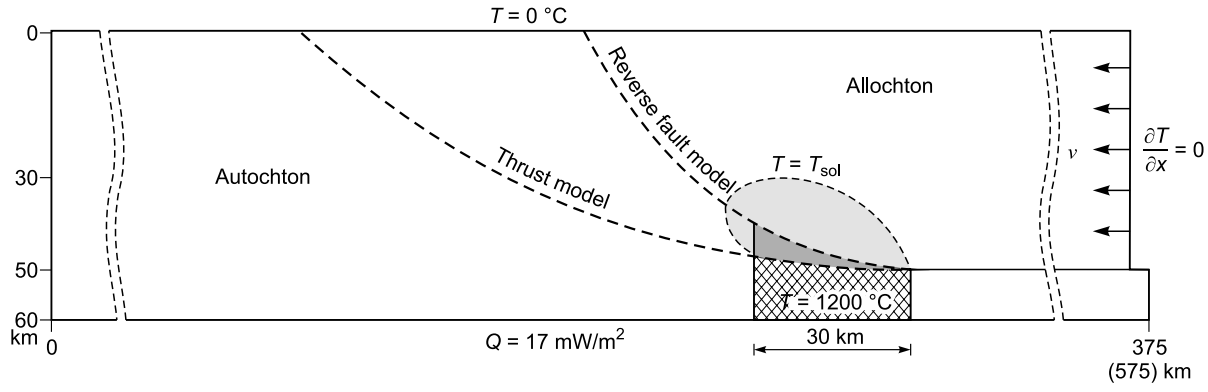

Fig. 10. Statement of problem of modeling the thermomechanical interaction of the Gorny Altai and West Sayan blocks during collisions and thermal impact of a deep-seated magma intrusion. The cross section of the 2D model corresponds to the SW-SW section across the Teletsk-Chulyshman metamorphic belt, see tectonic scheme in Fig. 1*b*. The initial structure of the collision zone is given in two versions of the model: (*1*) with a dip-slip (uplift) fault, (*2*) with a low-angle thrust. Hatching and dark gray tone shows the supposed basic magmatic intrusions at the crustal base. A light gray tone shows the partially molten region dynamically changing during the collision process. The horizontal size of the model area is 375 km (reverse fault model) and 575 km ("thrust" model).

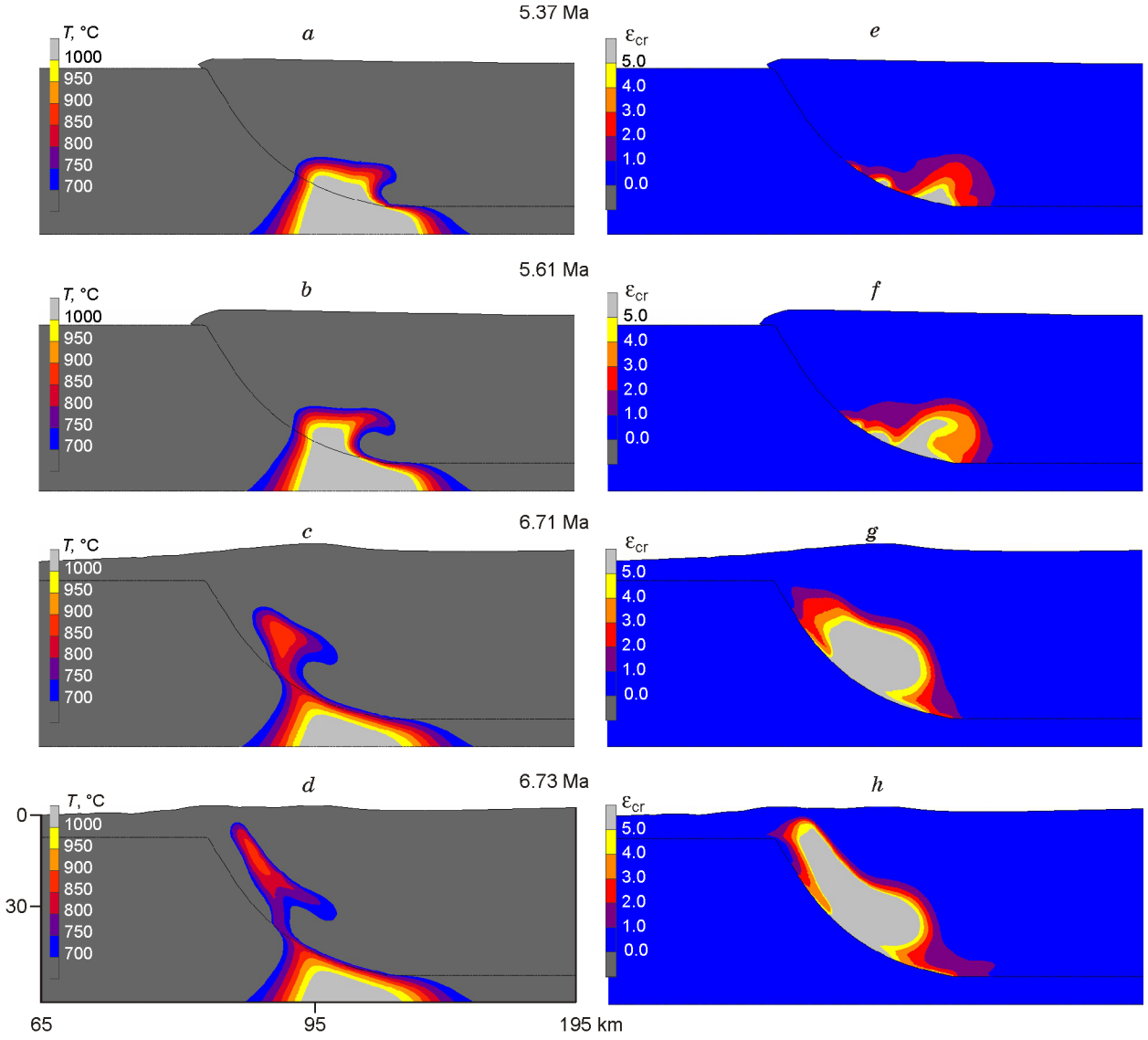

Fig. 11. Results of the collision simulation ("reverse fault" model) obtained for the total convergence rate of 5 cm/year. The enlarged central area of the model is shown. *a–d*, Temporal evolution of the temperature in the time interval 5.37–6.63 Myr (temperature scale bar is in range of 700–1000 °C); temperature region above 700 °C corresponds to the anatexis zone; *e–h*, temporal evolution of viscous deformations. Evolution times are indicated. Snapshots of strain in the range of (0–5) 100% are shown. Gray regions are correspond to maximum strain.

from the hot source and displaced together with the lower crustal matter due to thrust tectonics. As the upward movement continues, the migmatite body changes its shape within the rising medium and gradually cools down. The effect of crustal deformation on temperature field is quite significant in case of a steep thrust, according to the modeling results. The lower crustal matter of the Chulyshman block near the basic magma chamber is heated to 920–950 °C. In process of convergence (about 6.7 Ma, Fig. 11*d*), the anatexis front moves up to the depth of about 9 km. The high-temperature zone outlined by the isotherm of 700 °C narrows down towards the top and is controlled by the detachment plane position.

The model with gentler thrust is considered in more detail at various collision rates of blocks: 3, 5, 6, and 10 cm/yr. The maximum rise of the isotherm of 700 °C, the size of the high-temperature zone, and horizontal displacement of its center from the thermal source act as the comparison criteria for the models. The maximum temperature in the thrusted block at the collision rate of 3 cm/yr does not exceed 600 °C, and the isotherm $T = 600$ °C reaches the depth of 15 km. The temperature of 750 °C is reached at collision rates of 5, 6, and 10 cm/yr, which corresponds to peak metamorphism temperatures of the TCMB. The height of the uplift (h), the size (d), and the horizontal displacement (s) of the high-temperature anomaly are as follows: h =

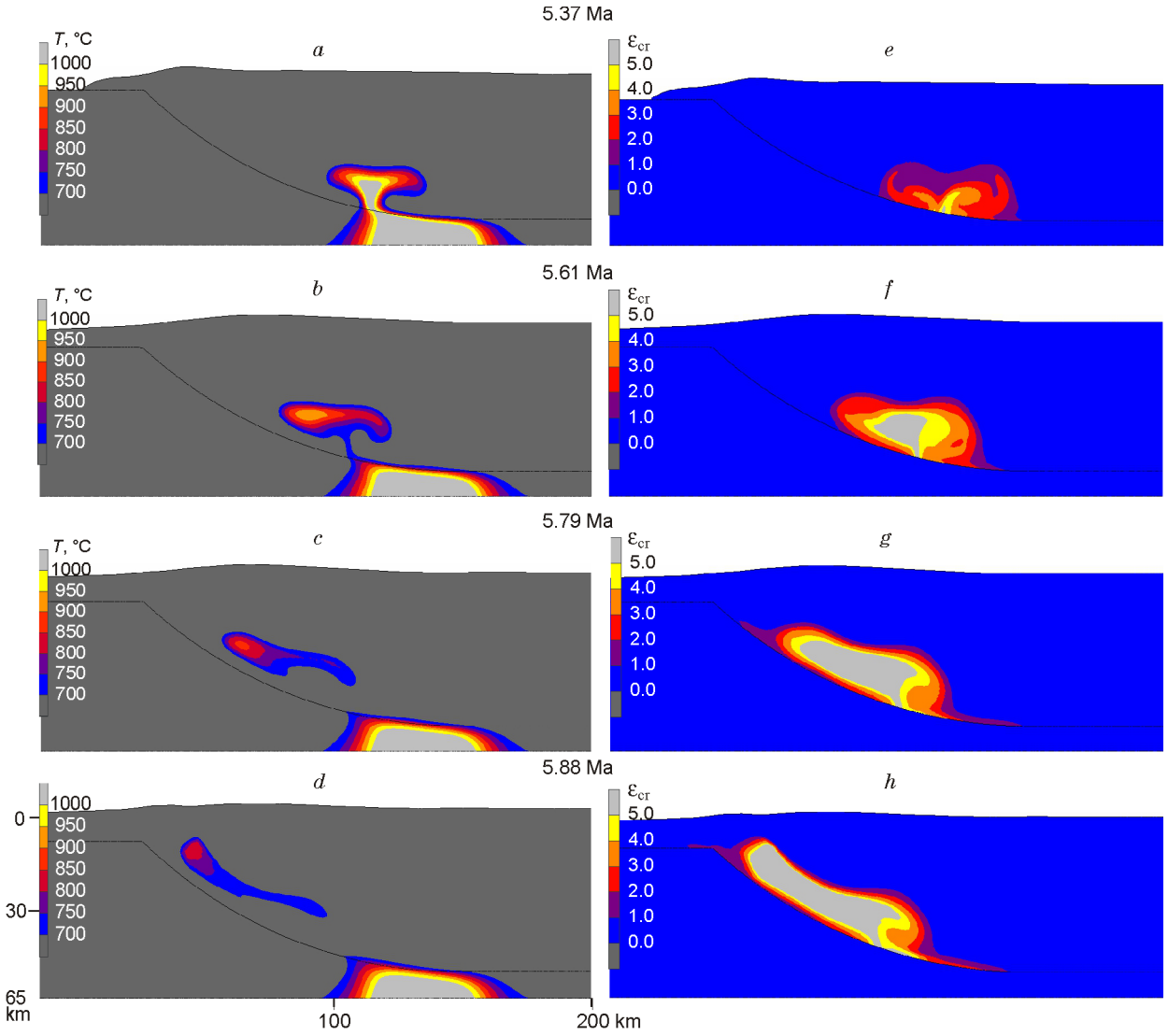

Fig. 12. Results of the collision simulation ("thrust" model) obtained for the total convergence rate of 10 cm/year. See caption for Fig. 11 for details.

30 km, d = 8 km, s = 64 km at the collision rate of 5 cm/yr, h = 17 km, d = 9 km, s = 85 km at 6 cm/yr, and h = 10 km, d = 10 km, s = 93 km at 10 cm/yr. These sets of values correspond to different points in time, specifically 6.49, 6.39, and 5.88 Ma.

The results for the thrust model with the collision rate of 10 cm/yr are represented in Fig. 12 through the evolution of viscous deformations and the temperature field. At the initial stage, a partially molten body is formed represented by the diapir, which is then detached from the magamtic thermal source (Fig. 12*b*, 5.6 Ma). High-temperature anomaly is sized 45 × 12 km (width and height). Collision leads to the displacement of the migmatite body from the magmatic chamber along the thrust, while the high-temperature zone shrinks, as it moves along the thrust. The migmatites formed at the depth are "frozen in" in the medium and move upwards together with the crustal matter and gradually crystallize, while preserving the high-temperature core size of about 10 km at the distance of 93 km from the thermal source (Fig. 12*d*, 5.88 Ma). A significant rise of the migmatization/anatexis front is explained by high collision rate and large deformations of the TCMB crust. Creep strain pattern is controlled by temperature distribution in the moving block. A sharp front of intense strain arises, which limits the low—viscosity area. According to the 2D model, this area is shaped as a channel parallel to the thrust, along which high-temperature matter moves (Fig. 12*g*–*h*). The channel boundary approximately matches the isotherm of 450 °C. The intense deformation area includes the anatectic melting zone bounded by the solidus front of wet granite (650–700 °C).

In addition, the calculation was performed with a magmatic chamber size reduced to 10 km at the collision rate of 10 cm/yr. This model showed a significantly smaller size and life span of the high-temperature zone ($T \geq 700$ °C),

than in the variant showed in Fig. 12. The front of the 700 °C isotherm only rises to the depth of about 25 km.

While comparing the modeling results at different thrust dipping and collision rates (Figs. 11 and 12), it is important to note that the anatexis front is able to travel upwards together with the lower crustal matter at collision rates of 5 cm/yr and above (Fig. 12). At lower rates (3 cm/yr and below), cooling occurs faster, than the uplift of the crust matter via obduction. Thus, the gentle thrust model is the best fit for the high-temperature metamorphism parameters observed in the TCMB.

DISCUSSION OF THE RESULTS

Validation of geodynamic conditions of the TCMB formation is discussed in multiple papers and still remains an unresolved problem. Based on phengite and glaucophane dating, the blueschist metamorphism age of the Uimon series is determined, and an Early Ordovician subduction stage is identified within the range of 491–484 Ma (Volkova et al., 2005; Volkova and Sklyarov, 2007). It should be noted that, according to the geological-geodynamic scheme of Gorny Altai (Buslov et al., 2013; Dobretsov et al., 2017), the Uimon zone is 170–180 km to the SW away from the Teletskoe–Chulyshman complex. They are separated by numerous faults, tectonic blocks of various origins (magmatic arc, Anyui–Chuya fore-arc trough, and back-arc basin) and is located almost on the opposite side of the Charysh–Terekta–Ulagan suture fault zone. To assume that the whole E–W section of the tectonic collage of Gorny Altai is a single subduction zone would be unlikely. The considered age stage is recognized in the papers (Dobretsov and Buslov 2007), where three critical orogenic stages are identified in the development of the Eurasian continental crust, i.e., late Cambrian–Ordovician (510–470 Ma), Late Devonian–early Carboniferous (380–320 Ma), and Permian–Triassic (285–230 Ma). The considered late Cambrian–Ordovician accretion-collision events occurred at the margin of the Altai–Mongolian microcontinent, and, according to the geodynamic scheme of Gorny Altai (Buslov et al., 2013), the TCMB belongs to its margin as well. Therefore, since no blueschists are observed in the TCMB, which are typical for the subduction zones, we assume that collision of continental margin blocks took.

The main detrital zircon population from metasedimentary rocks of the Ulagan (Bashkaus) complex, which is the closest one to the Chulyshman complex, matches the age range of 620–500 Ma (Chen et al., 2016). These datings are consistent with the later age of metamorphic zircon from migmatites of the Chulyshman complex of 484 Ma and leave a possibility for a thermal event to occur in this period. The presence of detrital zircon populations aged 480–460 Ma in other areas of the Chinese and Mongolian Altai (Chen et al., 2014a,b, 2015; Cai et al., 2016) probably indicates a slightly later protolith formation, but it is preferable to rely on the data from the closest region. It is worth noting that the studied zircons of the Chulyshman block of the TCMB do not contain detrital nuclei and possibly indicate the one-act crystallization during the metamorphic event.

Finding the actual thermal source that caused the anatexis and high-temperature metamorphism of the TCMB rocks is an important problem. Various possible causes of anatexis and formation of HT/LP metamorphic complexes in collisional orogenic structures are considered:

(1) Thickening of the radiogenic heat producing crust layers (England and Thompson, 1984; Gerdes et al., 2000).

(2) Anatexis and migmatization in orogenic belts is considered to be the result of pelite melting in the burial process during underthrusting (Brown, 2013). The magmatic heat source is absent in this model, and partial melting is assumed to be the result of water fluid release during dehydration of water-bearing minerals. Thus, the migmatite front, which tracks the solidus, is progressively extended into shallower parts of the orogenic system by advection of material during convergence thickening.

(3) Intrusion of basic magma into the base of the crust (underplating) in process of orogenic destruction (Kelsey and Hand, 2015). A basic intrusive chamber is assumed to be the thermal source in a number of cases. It is formed at the base of the crust as a result of underplating and then initiates melting, upward movement of felsic magma, and formation of wide contact aureoles (Olivier et al., 2004; Polyansky et al., 2012, 2016). Basic magmatism is usually associated with activity of spreading/rifting zones or hot spots. However, the recently obtained isotopic geochronology data indicate the synchronism of collision and basic magmatism. The latter was identified as a thermal source of metamorphism for collisional orogenic belts in a number of cases. Examples are assumed to be present in the Caledonian orogenic belt of Maine in the Appalachia (Thompson, 1984), the Connemara zonal complex in Ireland (Reverdatto and Polyansky, 2004), the Cambrian–Ordovician accretion-collision stage of West Sangilen massif (Shelepaev et al., 2018).

We use the latter of the listed mechanisms to explain the anatexis and formation of metamorphic complexes of the TCMB. However basic magma intrusion into the base of non-deforming crust is by itself insufficient to explain the rock heating conditions at shallow depths corresponding to pressures of 2.2–3.5 kbar. Models of conductive heating of immobile crust above the magmatic heat source with the initial temperature of 1200 °C at its base show that at the level of 2–3 kbar the heating does not exceed 400 °C. Thus, we propose the combined model of a simultaneous basic heat source and crust deformation under tectonic shortening and thrusting (a combination of mechanisms 2 and 3 from the list).

It is assumed that HT/MP metamorphism and anatexis in the Chulyshman Highlands area during the collision was caused by preceding deep basic magmatism. As mentioned

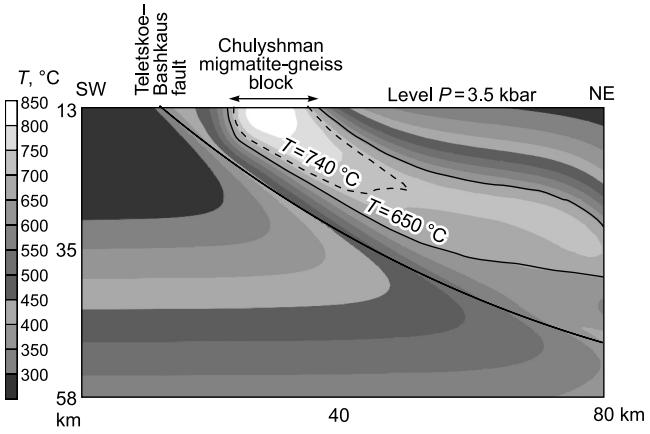

Fig. 13. Interpretation of the model results of the Chulyshman migmatite-gneiss complex formation in comparison with geothermobarometric estimates of the metamorphism parameters. Predicted temperature distribution is shown at the prograde stage, at the time of the maximum uplift of the Chulyshman migmatite-gneiss block to the level of P = 3.5 kbar (13 km). The isotherms 650 °C (the boundary of the migmatite body) and 740 °C (the temperature estimate from a mineral geothermometer) are highlighted by solid and dashed lines, respectively.

earlier, the heat source often cannot be identified from outcrops, since basic-ultrabasic intrusions are absent at the current erosion levels in many low-moderate pressure/high-temperature complexes and even UHT/granulite complexes (Kelsey and Hand, 2015). An example is described for the Tongulak metamorphic zoning within the Kurai complex, where zoning with anticlinal positioning of isograds was identified (Lepezin, 1972). The estimates based on geothermobarometry showed metamorphism parameters T = 650–670 °C, P = 3.5–5 kbar (Anan'ev et al., 2003). A basic intrusion at the depth of about 20 km represented by laccolith with wedge-like roof could act as a thermal source during metamorphic zoning formation. Comparison of P–T parameters of the TCMB and the Tongulak zonal complex makes it possible to assume that the former could have a significantly deeper magma chamber, but the heat transfer during thrusting in the TCMB resulted in heating of the rocks at shallower depths.

Remoteness of metamorphism products from the basaltic magmatic heat source may be explained by collisional movements along gentle thrusts. This evolutionary stage corresponds to accretion-collision events of the late Cambrian–Ordovician at the margin of the Altai–Mongolian microcontinent (Dobretsov and Buslov, 2007). Crustal rocks near basic intrusions are heated to anatectic temperatures, and migmatites are formed. As the deeply metamorphosed and partially molten matter moved upwards as a result of thrusting processes, it formed cores or 2D rollers similar to diapirs in structure, but with different formation mechanisms. Interpretation of modeling results of formation of the Chulyshman migmatite-gneiss complex is presented in Fig. 13. Temperature field is shown at the progressive stage, when the block is lifted to the highest level of P = 3.5 kbar (13 km). The age of 484 ± 6 Ma matches the rise of the solidus front and metamorphic aureole at the identified temperature of 740 °C to the lithostatic pressure level of 3.5 kbar. High thrust rate of 5–6 cm/yr and short duration of the upward movement within the range of 0.5–1.4 Ma ensure the conditions for transporting the matter in a partially melted state. The overall duration of the collision stage is probably significantly longer.

Model distributions of temperatures and viscous deformations confirm the cylindrical type of folding identified as a result of structural analysis. A similar example from the Chinese Altai, where the tectonic rise of migmatites to the level of 4–4.5 kbar took place during the formation of granite-gneiss cores, is described in (Jiang et al., 2015). Analog laboratory experiments (Ferre et al., 2012) confirm the possibility of simultaneous formation of thrusts and syn-kinematic intrusions with both basic and felsic compositions.

Thus, the formation of high-grade metamorphism under influence of heat from the basic magmatic chamber together with the uplift of heated matter along the gentle thrust seems to be the most realistic scenario for the TCMB. The developed thermal-mechanical model may also be used for other HT/LP complexes with high-grade metamorphism involving tectonic displacement from the magmatic heat source.

CONCLUSIONS

1. The obtained estimates of pressure (2.2–3.5 kbar) and temperature (about 740 °C) indicate an increased crustal thermal gradient of at least 60–90 °C/km in the region during the formation of the Teletskoe–Chulyshman metamorphic belt, which is typical for low-moderate pressure metamorphism conditions in the described metamorphic complexes of Gorny and Mongolian Altai (Anan'ev et al., 2003; Sukhorukov et al., 2016).

2. Metamorphism in the Chulyshman block is dated at 483.9 ± 5.7 Ma (Early Ordovician) based on U/Pb (SHRIMP) dating of zircons from migmatite gneisses. Moderate pressure/high-temperature metamorphism and anatexis in the block preceded the Early Ordovician metamorphism stage in the northern part of the TCMB, i.e., the Chul'cha block (466.7 ± 3.3 Ma (Gusev, 2013)).

3. The model implements a feasible mechanism, which agrees well with independent geothermobarometric estimates of metamorphism parameters. The modeling performed makes it possible to conclude that high-gradient metamorphism and anatexis, which accompany tectonic displacement of crustal blocks from the heat source, may lead to upward migration of partially melted previously subducted metasediments to upper crustal levels (up to pressures of 2.5–3.5 kbar). Migmatite-gneiss complexes may be placed away from the magmatic heat source in absence of direct hot contacts with the intrusion. The anatexis front movement rate during thrusting is found to be at least 6 cm/yr based on

the comparison of geothermobarometric estimates of metamorphism parameters with numerical modeling results[1].

It seems that understanding the nature of metamorphism would require detailed thermobarometric research of zonal minerals (particularly garnet) from metamorphic rocks of the Chul'cha block of the TCMB, as well as development of a thermal-mechanical numerical model taking into account longer duration and multiple stages of the collision process.

The work was supported by Sobolev Institute of Geology and Mineralogy, SB RAS under the state assignment, the Russian Foundation for Basic Research (project No. 17-05-00848), and by the Presidium of SB RAS under the integrative project no. 53. Mineralogical studies were performed at the Common Use Center of Multielement and Isotopic Research of Sobolev Institute of Geology and Mineralogy, SB RAS (Novosibirsk). Authors thank the reviewers N.L. Dobretsov and M.M. Buslov for constructive comments, N.I. Volkova for valuable consultations, I.S. Novikov, E.M. Vysotsky, S. Shevchenko of the Altai National Reserve (Yazula Lodge) for assistance in field research, and V.G. Sverdlova for help with figure processing.

REFERENCES

Anan'ev, V.A., Polyansky, O.P., Lepezin, G.G., Reverdatto, V.V., 2003. Metamorphic zoning of the Tongulak mountain range, Altai: mathematical modeling. Geologiya i Geofizika (Russian Geology and Geophysics) 44 (4), 297–304 (285–294).

Bhatia, M.R., Crook, K.A.W., 1986. Trace element characteristics of graywackes and tectonic setting discrimination of sedimentary basins. Contrib. Mineral. Petrol. 92 (2), 181–193.

Black, L.P., Kamo, S.L., Allen, C.M., Aleinikoff, J.N., Davis, D.W., Korsch, R.J., Foudoulis, C., 2003. TEMORA 1: a new zircon standard for Phanerozoic U–Pb geochronology. Chem. Geol. 200 (1–2), 155–170.

Blyuman, B.A., 1985. Endogenic Regimes and Metamorphism Types of Folded Areas [in Russian]. Nedra, Leningrad.

Brown, M., 2013. Granite: From genesis to emplacement. GSA Bull. 125, 1079–1113.

Buslov, M.M., 2011. Tectonics and geodynamics of the Central Asian Foldbelt: the role of Late Paleozoic large-amplitude strike-slip faults. Russian Geology and Geophysics (Geologiya i Geofizika) 52 (1), 52–71 (66–90).

Buslov, M.M., Watanabe, T., Smirnova, L.V., Fujiwara, I., Iwata, K., de Grave, J., Semakov, N.N., Travin, A.V., Kir'yanova, A.P., Kokh, D.A., 2003. Role of strike-slip faulting in Late Paleozoic–Early Mesozoic tectonics and geodynamics of the Altai–Sayan and East Kazakhstan regions. Geologiya i Geofizika (Russian Geology and Geophysics) 44 (1–2), 49–75 (47–71).

Buslov, M.M., Geng, H., Travin, A.V., Otgonbaatar, D., Kulikova, A.V., Chen, M., Stijn, G., Semakov, N.N., Rubanova, E.S., Abildaeva, M.A., Voitishek, E.E., Trofimova, D.A., 2013. Tectonics and geodynamics of Gorny Altai and adjacent structures of the Altai–Sayan folded area. Russian Geology and Geophysics (Geologiya i Geofizika) 54 (10), 1250–1271 (1600–1627).

Cai, K.D., Sun, M., Buslov, M.M., Jahn, B., Xiao, W., Long, X., Chen, H., Wan, B., Chen, M., Rubanova, E.S., Kulikova, A.V., Voytishek, E.E., 2016. Crustal nature and origin of the Russian Altai: Implications for the continental evolution and growth of the Central Asian Orogenic Belt (CAOB). Tectonophysics 674, 182–194.

Chen, M., Sun, M., Cai, K., Buslov, M.M., Zhao, G., Rubanova, E.S., 2014a. Geochemical study of the Cambrian–Ordovician meta-sedimentary rocks from the northern Altai–Mongolian terrane, northwestern Central Asian Orogenic Belt: Implications on the provenance and tectonic setting. J. Asian Earth Sci. 96, 69–83.

Chen, M., Sun, M., Cai, K., Buslov, M.M., Zhao, G., Rubanova, E.S., Voytishek, E.E., 2014b. Detrital zircon record of the early Paleozoic meta-sedimentary rocks in Russian Altai: Implications on their provenance and the tectonic nature of the Altai–Mongolian terrane. Lithos 233, 209–222.

Chen, M., Sun, M., Buslov, M.M., Cai, K., Zhao, G., Zheng, J., Rubanova, E.S., Voytishek, E.E., 2015. Neoproterozoic–middle Paleozoic tectono-magmatic evolution of the Gorny Altai terrane, northwest of the Central Asian Orogenic Belt: Constraints from detrital zircon U–Pb and Hf-isotope studies. Lithos 233, 223–236.

Chen, M., Min, S., Cai, K., Buslov, M.M., Zhao, G., Jiang, Y., Rubanova, E.S., Kulikova, A.V., Voytishek, E.E., 2016. The early Paleozoic tectonic evolution of the Russian Altai: Implications from geochemical and detrital zircon U–Pb and Hf isotopic studies of meta-sedimentary complexes in the Charysh–Terekta–Ulagan–Sayan suture zone. Gondwana Res. 34, 1–15.

Dobretsov, N.L., Buslov M.M., 2007. Late Cambrian–Ordovician tectonics and geodynamics of Central Asia. Russian Geology and Geophysics (Geologiya i Geofizika) 48 (1), 71–82 (93–108).

Dobretsov, N.L., Kirdyashkin, A.G., Kirdyashkin, A.A., 2001. Deep-Seated Geodynamics [in Russian]. ISO RAN, Novosibirsk.

Dobretsov, N.L., Buslov, M.M., Rubanova, E.S., Vasilevsky, A.N., Kulikova, A.V., Bataleva, E.A., 2017. Middle–Late Paleozoic geodynamic complexes and structure of Gorny Altai and their record in gravity data. Russian Geology and Geophysics (Geologiya i Geofizika) 58 (11), 1277–1288 (1617–1632).

England, P.C., Thompson, A.B., 1984. Pressure-temperature-time paths of regional metanlorphism: Heat transfer during the evolution of regions of thickened continental crust. J. Petrol. 25, 894–928.

Ferre, E.C., Galland, O., Montanari, D., Kalakay, T.J., 2012. Granite magma migration and emplacement along thrusts. Int. J. Earth Sci. 101 (7), 1673–1688.

Gerdes, A., Worner, G., Henk, A., 2000. Post-collisional granite generation and HT–LP metamorphism by radiogenic heating: the Variscan South Bohemian Batholith. J. Geol. Soc. 157 (3), 577–587.

Ghiorso, M.S., Evans, B.W., 2008. Thermodynamics of rhombohedral oxide solid solutions and a revision of the Fe–Ti two-oxide geothermometer and oxygen-barometer. Am. J. Sci. 308 (9), 957–1039.

Glorie, S., De Grave, J., Buslov, M.M., Zhimulev, F.I., Izmer, A., Vandoorne, W., Ryabinin, A., Van den Haute, P., Vanhaecke, F., Elburg, M.A., 2011. Formation and Palaeozoic evolution of the Gorny-Altai–Altai–Mongolia suture zone (South Siberia): Zircon U/Pb constraints on the igneous record. Gondwana Res. 20 (2–3), 465–484.

Gromet, L.P., Haskin, L.A., Korotev, R.L., Dymek, R.F., 1984. The "North American shale composite": Its compilation, major and trace element characteristics. Geochim. Cosmochim. Acta 48 (12), 2469–2482.

[1] To summarize the data obtained in the present paper and the concepts shared by the researchers of the region, the remaining unresolved problems regarding the evolution of metamorphism in the TCMB are to be mentioned. Nonuniformity of metamorphism manifests itself in the Chul'cha block, where, according to (Gusev, 2009), garnet is observed, which is confirmed by observations by M.M. Buslov and N.L. Dobretsov. According to M.M. Buslov and N.L. Dobretsov, the obtained geochronology makes it possible to identify two stages of metamorphism with peaks at 484 and 470 Ma. The second metamorphism stage matches the Early Ordovician stage determined earlier in the northern part of the TCMB, i.e., the Chul'cha block (466.7 Ma (Gusev, 2013)). According to M.M. Buslov and N.L. Dobretsov, the absence of the pronounced zoning in the TCMB and multistage deformations with peculiar laying folds contradicts the model of a one-act thermal-collision process of the TCMB formation.

Gusev, N.I., 2013. Metamorphic Complexes of Mountain Altai [in Russian]. Lambert Academic Publishing, Saarbrucken.

Jiang, Y.D., Stipska, P., Sun, M., Schulmann, K., Zhang, J., Wu, Q.H., Long, X.P., Yuan, C., Racek, M., Zhao, G.C., Xiao, W.J., 2015. Juxtaposition of Barrovian and migmatite domains in the Chinese Altai: a result of crustal thickening followed by doming of partially molten lower crust. J. Metamorph. Geol. 33, 45–70.

Johaness, W., Holts, F., 1996. Petrogenesis and Experimental Petrology of Granitic Rocks. Berlin, Springer.

Johnson, M.R.W., Harley, S.L., 2012. Orogenesis: The Making of Mountains. Cambridge Univ. Press, Cambridge.

Hansen, F.D., Carter, N.L., 1982. Creep of selected crustal rocks at 1000 MPa. Trans. Am. Geophys. Union 63, 437.

Harley, S.L., Kelly, N.M., Möller, A., 2007. Zircon behaviour and the thermal history of mountain chains. Elements 3, 25–30.

Herron, M.M., 1988. Geochemical classification of terrigenous sands and shales from core or log data. J. Sediment. Res. 58 (5), 820–829.

Holcombe, R.J., 2015. GEOrient v.9.5.1 User's Manual. 2015, http://www.holcombe.net.au/software/georient.html.

Kargopolov, S.A., Polyansky, O.P., Reverdatto, V.V., Novikov, I.S., Vysotsky, E.M., 2016. High-gradient metamorphism and anatexis in the Teletsk–Chulyshman metamorphic belt (Gornyi Altai): New data on the age and estimate of *P–T* parameters. Dokl. Earth Sci. 471 (1), 1174–1178.

Kelsey, D.E., Hand, M., 2015. On ultrahigh temperature crustal metamorphism: Phase equilibria, trace element thermometry, bulk composition, heat sources, timescales and tectonic settings. Geosci. Front. 6, 311–356.

Korobeinikov, S.N., Polyansky, O.P., Likhanov, I.I., Sverdlova, V.G., Reverdatto, V.V., 2006. Mathematical modeling of overthrusting fault as a cause of andalusite-kyanite metamorphic zoning in the Yenisei Ridge. Dokl. Earth Sci. 408 (4), 652–656.

Korobeinikov, S.N., 2000. Nonlinear Deformation of the Solids [in Russian]. ISO RAN, Novosibirsk.

Korobeinikov, S.N., Reverdatto, V.V., Polyanskii, O.P., Sverdlova, V.G., Babichev, A.V., 2012. Surface topography formation in a region of plate collision: Mathematical modeling. J. Appl. Mech. Tech. Phys. 53 (4), 577–588.

Korobeynikov, S.N., Polyansky, O.P., Sverdlova, V.G., Babichev, A.V., Reverdatto, V.V., 2008. Computer modeling of underthrusting and subduction under conditions of gabbro-eclogite transition in the mantle. Dokl. Earth Sci. 421 (1), 724–728.

Kruk, N.N., 2015. Continental crust of Gorny Altai: stages of formation and evolution; indicative role of granitoids. Russian Geology and Geophysics (Geologiya i Geofizika) 56 (8), 1097–1113 (1403—1423).

Kruk, N.N., Volkova, N.I., Kuybida, Y.V., Gusev, N.I., Demonterova, E.I., 2013. Nature of the metamorphic complexes of the Altai Mountains. Litosfera 2, 20–44.

Lepezin, G.G., 1972. Metamorphism of the Epidote-Amphibolite Facies on the Example of the Tongulak Complex (Gorny Altai) [in Russian]. Nauka, Moscow.

Likhanov, I.I., Polyansky, O.P., Reverdatto, V.V., Memmi, I., 2004. Evidence from Fe- and Al-rich metapelites for thrust loading in the Transangarian region of the Yenisey Ridge, eastern Siberia. J. Metamorph. Geol. 22 (8), 743–762.

Ludwig, K.R., 2000. SQUID1.00 A User's Manual. Berkeley Geochr. Cent. Spec. Publ., Vol. 2.

McLennan, S.M., Hemming, S., McDaniel, D.K., Hanson, G.N., 1993. Geochemical approaches to sedimentation, provenance and tectonics, in: Johnsson, M.J., Basu, A. (Eds.), Processes Controlling the Composition of Clastic Sediments. GSA Spec. Pap. 284. Boulder, pp. 21–40.

Miller, Yu.V., 1982. Tectonic-Metamorphic Cycles [in Russian]. Nauka, Leningrad.

Nesbitt, H.W., Young, G.M., 1982. Early Proterozoic climates and plate motions inferred from major element chemistry of lutites. Nature 299, 715–717.

Nokleberg, W.J., Badarch, G., Berzin, N.A., Diggles, M.F., Hwand, D.H., Khanchuk, A.I., Miller, R.J., Naumova, V.V., Obolensky, A.A., Ogasawara, M., Parfenov, L.M., Prokopiev, A.V., Rodionov, S.M., Yan, H., 2004. Northeast Asia Geodynamics, Mineral Deposits Location, and Metallogenic Maps. USGS Open-File Report 2004-1252.

Olivier, Ph., Gleizes, G., Paquette, J.L., 2004. Gneiss domes and granite emplacement in an obliquely convergent regime: New interpretation of the Variscan Agly Massif (Eastern Pyrenees, France), in: Whitney, D.L., Teyssier, C., Siddoway, C.S. (Eds.), Gneiss Domes in Orogeny. GSA Spec. Pap. 380, pp. 229–242.

Passchier, C.W., Trouw, R.A.J., 2005. Microtectonics. Springer, Berlin.

Pattison, D.R.M., 1992. Stability of andalusite and sillimanite and the Al_2SiO_5 triple point: constraints from the Ballachulish aureole. Scot. J. Geol. 100. 423–446.

Pattison, D.R.M., Chako, T., Farquhar, J., McFarlane, C.R.M., 2003. Temperatures of granulite-facies metamorphism: constraints from experimental phase equilibria and thermobarometry corrected from retrograde exchange. J. Petrol. 44 (5), 867–900.

Polyansky, O.P., Korobeynikov, S.N., Sverdlova, V.G., Babichev, A.V., Reverdatto, V.V., 2010. The influence of crustal rheology on plate subduction based on numerical modeling results. Dokl. Earth Sci. 430 (2), 158–162.

Polyansky, O.P., Korobeynikov, S.N., Babichev, A.V., Reverdatto, V.V. 2012. Formation and upwelling of mantle diapirs through the cratonic lithosphere: Numerical thermomechanical modeling. Petrology 20 (2), 120–137.

Polyansky, O.P., Korobeynikov, S.N., Babichev, A.V., Reverdatto, V.V., Sverdlova, V.G., 2014. Numerical modeling of mantle diapirism as a cause of intracontinental rifting. Izvestiya, Phys. Solid Earth 50 (6), 839–852.

Polyansky, O.P., Babichev, A.V., Sukhorukov, V.P., Zinoviev, S.V., Reverdatto, V.V., 2015. A Thermotectonic Numerical Model of Collisional Metamorphism in the Mongolian Altai. Dokl. Earth Sci. 465 (1), 1164–1167.

Polyansky, O.P., Reverdatto, V.V., Babichev, A.V., Sverdlova, V.G., 2016. The mechanism of magma ascent through the solid lithosphere and relation between mantle and crustal diapirism: numerical modeling and natural examples. Russian Geology and Geophysics (Geologiya i Geofizika) 57 (6), 843–857 (1073–1091).

Prokoph, A., Ernst, R.E., Buchan, K.L., 2004. Time-series analysis of large igneous provinces: 3500 Ma to present. J. Geol. 112 (1), 1–22.

Quick, J.E., Sinigoi, S., Mayer, A., 1994. Emplacement dynamics of a large mafic intrusion in the lower crust, Ivrea-Verbano Zone, northern Italy. J. Geophys. Res. 99, 21,559–21,573.

Ranalli, G., 1995. Rheology of the Earth. Chapman & Hall, London, p. 413.

Reverdatto, V.V., Polyansky, O.P., 1992. Evolution of PT-parameters in the alternative models of metamorphism. Dokl. RAN 325 (5), 1017–1020.

Reverdatto, V.V., Polyansky, O.P., 2004. Modelling of the thermal history of metamorphic zoning in the Connemara region (western Ireland). Tectonophysics 379 (1–4), 77– 91.

Reverdatto, V.V., Likhanov, I.I., Polyansky, O.P., Sheplev, V.S., Kolobov, V.Yu. (Eds.), 2019. The Nature and Models of Metamorphism. Springer Geology, Switzerland, Cham.

Roser, B.P., Korsch, R.J., 1986. Determination of tectonic setting of sandstone-mudstone suites using SiO_2 content and K_2O/Na_2O ratio. J. Geol. 94 (5), 635–650.

Roser, B.P., Korsch, R.J. 1988. Provenance signatures of sandstone-mudstone suites determined using discriminant function analysis of major-element data. Chem. Geol. 67 (1–2), 119–139.

Rubatto, D., 2002. Zircon trace element geochemistry: Partitioning with garnet and the link between U–Pb ages and metamorphism. Chem. Geol. 184 (1–2), 123–138.

Rudnev, S.N., Vladimirov, A.G., Ponomarchuk, V.A., Kruk, N.N., Babin, G.A., Borisov, S.M., 2004. Early Paleozoic granitoid batho-

liths of the Altai–Sayan folded region (Lateral-temporal zoning and sources). Dokl. Earth Sci. 396 (4), 492–495.

Shelepaev, R.A., Egorova, V.V., Izokh, A.E., Seltmann, R., 2018. Collisional mafic magmatism of the fold-thrust belts framing southern Siberia (Western Sangilen, southeastern Tuva). Russian Geology and Geophysics (Geologiya i Geofizika) 59 (5), 525–540 (653–672).

Shokalskii, S.P., Babin, G.A., Vladimirov, A.G., Borisov, S.M., 2000. Correlation of Magmatic and Metamorphic Complexes of the Western Part of the Altai–Sayan Folded Region [in Russian]. Akad. Izd. Geo, Novosibirsk.

Shokal'skii, S.P., Turkin, Yu.A., Fedak, S.I. (Eds.), 2011. State Geological Map of the Russian Federation at a Scale of 1: 1,000,000 (Sheet M-45 Gorno-Altaisk) [in Russian]. VSEGEI, St. Petersburg.

Sukhorukov, V.P., Polyansky, O.P., Krylov, A.A., Zinoviev, S.V., 2016. Reconstruction of the metamorphic P–T path from the garnet zoning in aluminous schists from the Tsogt Block, Mongolian Altai. Petrology 24 (4), 409–432.

Taylor, S.R., McLennan, S.M., 1985. The Continental Crust: Its Composition and Evolution. Oxford, Blackwell.

Thompson, J.F.H., 1984. Acadian synorogenic mafic intrusions in the Maine Appalachians. Am. J. Sci. 284 (4–5), 462–483.

Vladimirov, A.G., Kruk, N.N., Khromykh, S.V., Polyansky, O.P., Chervov, V.V., Vladimirov, V.G., Travin, A.V., Babin, G.A., Kuibida, M.L., Khomyakov, V.D., 2008. Permian magmatism and lithospheric deformation in the Altai caused by crustal and mantle thermal processes. Russian Geology and Geophysics (Geologiya i Geofizika) 49 (7), 468–479 (621–636).

Volkova, N.I., Sklyarov, E.V., 2007. High-pressure complexes of Central Asian Fold Belt: geologic setting, geochemistry, and geodynamic implications. Russian Geology and Geophysics (Geologiya i Geofizika) 48 (1), 83–90 (109–119).

Volkova, N.I., Stupakov, S.I., Tret'yakov, G.A., Simonov, V.A., Travin, A.V., Yudin, D.S., 2005. Blueschists from the Uimon Zone as evidence of Ordovician accretionary-collisional events in Gorny Altai. Geologiya i Geofizika (Russian Geology and Geophysics) 46 (4), 367–382 (361–378).

Williams, I.S., 1998. U–Th–Pb geochronology by ion microprobe, in: McKibben, M.A., Shanks III W.C., Ridley, W.I. (Eds.), Rev. Econ. Geol., Vol. 7, pp. 1–35.

Yudovich, Ya.E., Ketris, M.P., 2000. Basics of Lithochemistry [in Russian]. Nauka, Leningrad.

Editorial responsibility: N.L. Dobretsov